HHS Public Access

Author manuscript

Cell Rep. Author manuscript; available in PMC 2024 October 23.

Published in final edited form as:

Cell Rep. 2020 September 01; 32(9): 108104. doi:10.1016/j.celrep.2020.108104.

An Epilepsy-Associated *GRIN2A* Rare Variant Disrupts CaMKIIα Phosphorylation of GluN2A and NMDA Receptor Trafficking

Marta Mota Vieira[1], **Thien A. Nguyen**[1], **Kunwei Wu**[2], **John D. Badger II**[1], **Brett M. Collins**[3], **Victor Anggono**[4], **Wei Lu**[2], **Katherine W. Roche**[1,5,*]

[1]Receptor Biology Section, National Institute of Neurological Disorders and Stroke (NINDS), National Institutes of Health (NIH), Bethesda, MD 20892, USA

[2]Synapse and Neural Circuit Research Section, NINDS, NIH, Bethesda, MD 20892, USA

[3]Institute for Molecular Bioscience, University of Queensland, St Lucia, QLD 4072, Australia

[4]Clem Jones Centre for Ageing Dementia Research, Queensland Brain Institute, University of Queensland, St Lucia, QLD 4072, Australia

[5]Lead Contact

SUMMARY

Rare variants in *GRIN* genes, which encode NMDAR subunits, are strongly associated with neurodevelopmental disorders. Among these, *GRIN2A*, which encodes the GluN2A subunit of NMDARs, is widely accepted as an epilepsy-causative gene. Here, we functionally characterize the *de novo* GluN2A-S1459G mutation identified in an epilepsy patient. We show that S1459 is a CaMKIIα phosphorylation site, and that endogenous phosphorylation is regulated during development and in response to synaptic activity in a dark rearing model. GluN2A-S1459 phosphorylation results in preferential binding of NMDARs to SNX27 and a corresponding decrease in PSD-95 binding, which consequently regulates NMDAR trafficking. Furthermore, the epilepsy-associated GluN2A-S1459G variant displays defects in interactions with both SNX27 and PSD-95, resulting in trafficking deficits, reduced spine density, and decreased excitatory synaptic transmission. These data demonstrate a role for CaMKIIα phosphorylation of GluN2A in receptor targeting and implicate NMDAR trafficking defects as a link to epilepsy.

Graphical Abstract

*Correspondence: rochek@nih.gov.

AUTHOR CONTRIBUTIONS

M.M.V. and K.W.R. designed the study. M.M.V. and T.A.N. performed the biochemical and imaging experiments. K.W. and W.L. designed and performed the electrophysiology experiments. J.D.B. provided experimental support. B.M.C. and V.A. provided research tools and scientific input. K.W.R. supervised the project. M.M.V. wrote the manuscript, with contributions and edits from all of the authors.

SUPPLEMENTAL INFORMATION

Supplemental Information can be found online at https://doi.org/10.1016/j.celrep.2020.108104.

DECLARATION OF INTERESTS

The authors declare no competing interests.

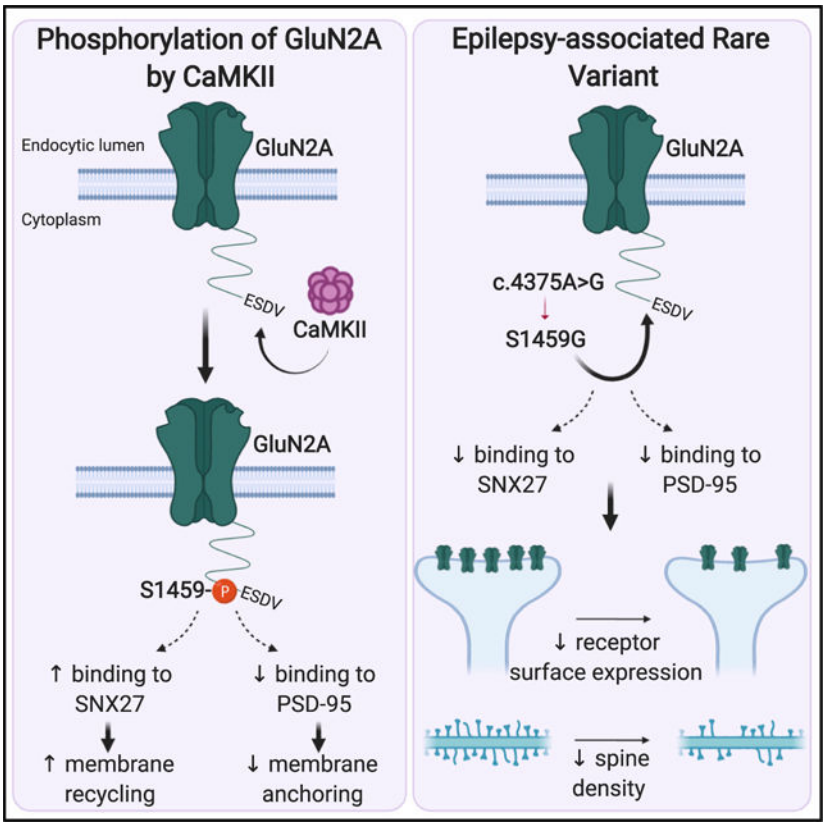

In Brief

Mota Vieira et al. identify CaMKII phosphorylation of the GluN2A subunit on S1459 as a mechanism regulating NMDAR trafficking. An epilepsy-associated rare variant at this same residue, GluN2A-S1459G, results in altered protein interactions, decreased NMDAR surface expression, and reduced synaptic function, providing potential insight into an epilepsy phenotype.

INTRODUCTION

N-Methyl-D-aspartate receptors (NMDARs) are critical players in glutamatergic transmission, synaptic plasticity, and neuronal development. Given their central roles, their dysfunction has been implicated in a variety of neurological disorders (Endele et al., 2010; Zhou and Sheng, 2013). With the advancement of sequencing technologies, genetic patterns underlying neurodevelopmental disorders have started to emerge, revealing that a cluster of synaptic genes is responsible for disease etiology in a subset of epilepsy, autism spectrum disorders (ASDs), and intellectual disability (ID) patients (Gilman et al., 2011; Satterstrom et al., 2020; Willsey et al., 2018). In particular, NMDAR subunits have been found to be highly correlated with neurodevelopmental disorders, with a plethora of rare variants identified in genetic screens (Carvill et al., 2013; Lesca et al., 2013, 2019; Tarabeux et al., 2011). Notably, the *GRIN2B* gene, which encodes the GluN2B subunit, is now considered to be one of the top ASD-associated genes (Platzer and Lemke, 2018; Sanders et al., 2015), whereas *GRIN2A*, which encodes the GluN2A subunit, is strongly linked to diseases

in the epilepsy spectrum (Lemke et al., 2013; Myers and Scheffer, 2016; Myers et al., 2019). In fact, *GRIN2A* is now classified in the OMIM database as the causative gene for focal epilepsy with speech disorder. Despite the strong genetic link between *GRIN* genes and neurodevelopmental disorders, the underlying functional consequences remain largely obscure. A few recent studies have provided interesting insights into the biology of receptors harboring epilepsy patient variants. The effects range from loss-of-function effects, such as decreased surface expression and impaired agonist-evoked currents, to gain-of-function effects leading, for example, to increased agonist potency (Sibarov et al., 2017; Strehlow et al., 2019; Yuan et al., 2014). Notably, most of the functional analyses of *GRIN2A* variants have focused on the assessment of mutations that affect residues in the agonist binding and channel portions of the receptor, which translate into either hyper- or hypofunction of NMDARs. The mechanisms of dysfunction elicited by mutations in the intracellular domain of the subunits, however, have remained largely understudied.

The GluN2A and GluN2B subunits are two of the most abundant NMDAR subunits in the forebrain, forming diheteromeric or triheteromeric complexes with the obligatory GluN1 subunit (Al-Hallaq et al., 2007; Cull-Candy and Leszkiewicz, 2004; Hansen et al., 2014; Sheng et al., 1994). Different subunit compositions fine-tune NMDARs in terms of intracellular protein interactions, localization in the synaptic membrane, and channel properties (reviewed by Vieira et al., 2020). Relative to GluN2B, the GluN2A subunit confers distinct receptor properties, including faster kinetics, lower glutamate affinity, greater channel open probability, and more prominent Ca^{2+}-dependent desensitization (Cull-Candy and Leszkiewicz, 2004; Wyllie et al., 2013). The GluN2A and GluN2B subunits share a high degree of similarity in their extracellular (including the ligand-binding domain) and transmembrane domains, suggesting a conserved function for these regions in both subunits. The C-terminal domain (CTD), however, is the most divergent region among these subunits, with only 29% identity between GluN2A and GluN2B (Ryan et al., 2013). This region enables NMDARs to interact with diverse intracellular proteins and links the receptors to downstream signaling pathways. A variety of phosphorylation events have been identified in the CTD of GluN2A/B subunits that modulate receptor properties (reviewed by Sanz-Clemente et al., 2013b). One of the most prominently studied kinases in the context of synaptic function is Ca^{2+}/calmodulin-dependent protein kinase II (CaMKII), which plays essential roles in synaptic plasticity (Bayer and Schulman, 2019; Shonesy et al., 2014) and regulates NMDARs, both via its kinase activity and by exerting structural roles (Barria and Malinow, 2005; Incontro et al., 2018; Sanhueza et al., 2011).

Most NMDARs localize to the postsynaptic density (PSD), which consists of a complex web of scaffolding, adaptor, and signaling proteins. Glutamate receptors have been shown to undergo rapid synaptic exchange (Tovar and Westbrook, 2002) and to diffuse between synaptic and extrasynaptic sites (Groc et al., 2004). In the spine, NMDARs interact with a variety of proteins, including members of the membrane-associated guanylate kinase (MAGUK) family (Won et al., 2017), such as PSD-95. These scaffolds act as organizers of the PSD, coupling signaling complexes to receptor function. NMDAR subunits are also regulated via interactions with endocytic proteins. Among these, sorting nexin-27 (SNX27), a member of the large protein family of sorting nexins, modulates NMDAR trafficking events (Clairfeuille et al., 2016; Wang et al., 2013). This is the only member of the SNX

family to contain a PDZ domain (Cullen, 2008), allowing potential interactions with PDZ-binding domain-containing proteins, such as NMDAR subunits.

In this work we investigated the functional effects of a GluN2A rare variant, GluN2A-S1459G (reported in ClinVar: VCV000224108.1; Bowling et al., 2017). We determined that GluN2A-S1459 is a CaMKIIα phosphorylation site. Using a combination of biochemistry and imaging assays, we demonstrated endogenous GluN2A-S1459 phosphorylation, which is regulated during development and in response to light in the visual cortex. GluN2A-S1459 phosphorylation dictates binding to SNX27 versus PSD-95, and consequently receptor trafficking. The epilepsy-associated variant abolishes any phosphorylation event and inhibits binding to both SNX27 and PSD-95. Moreover, we observed defects in NMDAR trafficking when comparing the GluN2A-S1459G to wild type (WT), as well as a decrease in spine density and miniature excitatory postsynaptic currents (mEPSCs). Thus, we observed altered receptor trafficking and synaptic defects, which may contribute to disease etiology. We conclude that GluN2A-S1459 is an important determinant for receptor modulation, in the establishment of protein-protein interactions via the PDZ-binding domain of GluN2A, and in the regulation of receptor levels at the cell surface, in particular during development.

RESULTS

GluN2A Is Phosphorylated by CaMKIIα at S1459

The *GRIN2A* gene that encodes GluN2A has numerous disease-associated variants in epilepsy patients (Carvill et al., 2013; Lesca et al., 2013, 2019). Whereas variants in the ligand-binding and transmembrane domains of the subunit are likely to affect receptor channel properties and folding, variants in the CTD probably result in defects in receptor trafficking, protein-protein interactions, and stability at the synapse. We set out to determine the effects of the *de novo* mutation *GRIN2A* c.4375A>G, that results in the missense variant GluN2A-S1459G, identified in a focal epilepsy patient with a speech disorder (ClinVar; Bowling et al., 2017). Notably, this variant is absent from the normal population, which indicates that it is potentially disease causing (gnomAD database, verified on July 6, 2020). In addition, this residue is highly conserved across species and in all four human GluN2 subunits (Figure 1A), which suggests that this site is under evolutionary constraint against variation.

We first recognized that this variant affected a serine, which may be a target for phosphorylation. GluN2A-S1459 has been identified as a target of *in vivo* phosphorylation in several recent phosphoproteomic studies (Goswami et al., 2012; Munton et al., 2007; Trinidad et al., 2006; Tweedie-Cullen et al., 2009), although the putative kinase is unknown. Furthermore, phosphorylation sites in the vicinity of the PDZ-binding domain of a variety of postsynaptic proteins dictate protein binding, trafficking, and synaptic localization (Clairfeuille et al., 2016; Cohen et al., 1996; Jeong et al., 2019; Roche et al., 2001; Sanz-Clemente et al., 2010). We reasoned that if GluN2A-S1459 is phosphorylated, then disruption of this post-translational modification (PTM) may underlie deficits in the disease-associated GluN2A-S1459G variant. To test this hypothesis, we characterized the putative phosphorylation of GluN2A-S1459. We performed *in vitro* kinase assays with candidate kinases (protein kinase A [PKA], PKC, and CaMKIIα) (Figures 1B, 1C, and S1). We

identified CaMKIIα as the relevant kinase that targets this site, because we detected a robust phosphorylation signal in the WT condition that was completely ablated in the S1459A condition. We observed this in both the ^{32}P-ATP *in vitro* assay (Figure 1B) and the immunoblot analysis using a phosphospecific antibody (Figure 1C). Notably, we did not observe such an effect when we tested PKC or PKA (Figure S1). To validate CaMKIIα as the specific kinase responsible for this phosphorylation event *in situ*, we expressed full-length GluN2A, GluN1, and CaMKIIα (either the WT, the K42R kinase dead mutant, or the T286D autonomously active mutant) in HEK293T cells and probed for the phosphorylation of GluN2A-S1459 (Figure 1D). GluN2A was phosphorylated by both WT and T286D CaMKIIα. However, when co-expressed with the kinase dead mutant, the level of GluN2A-S1459 phosphorylation was significantly reduced. The specificity of the antibody was confirmed by the absence of signal when probing lysates from cells co-expressing the phospho-dead mutant GluN2A-S1459A. We also found that GluN2A-S1459 is endogenously phosphorylated in mouse brain. The fractionation of adult mouse brains indicates that GluN2A-phosphoS1459 is enriched in the PSD (Figure 1E). Finally, as an additional control, we treated PSD fractions from WT brains with λ-phosphatase and observed a reduction in the phosphor-GluN2A signal (Figure 1F). We therefore demonstrated endogenous phosphorylation of GluN2A-S1459, which is likely mediated by CaMKIIα, although we cannot exclude the role of other serine/ threonine kinases in this phosphorylation event *in vivo*.

The Phosphorylation of GluN2A-S1459 Is Developmentally Regulated

NMDARs undergo a well-characterized GluN2B-to-GluN2A subunit switch during development, which occurs around the second post-natal week in rodents (Hestrin, 1992, Monyer et al., 1994, Sanz-Clemente et al., 2013a). To better understand the endogenous role of this PTM, we analyzed the developmental profile of GluN2A-S1459 phosphorylation. We observed a peak of phosphorylated GluN2A between P7 and P11 in PSD fractions of WT mouse brains (Figures 2A and 2B), which precedes the subunit switch. This profile is provocative, suggesting that the phosphorylation of GluN2A at S1459 may enhance the targeting of GluN2A to the synapse, where NMDARs containing GluN2A partially replace the GluN2B receptors by the second post-natal week, thereby contributing to synapse maturation in the mouse brain.

Synaptic activity promotes the surface delivery of GluN2A-containing NMDARs (Barria and Malinow, 2002; Bellone and Nicoll, 2007). To test whether activity can modulate the phosphorylation of GluN2A-S1459, we performed dark-rearing experiments, a well-established *in vivo* activity paradigm that induces changes in the visual cortex (Carmignoto and Vicini, 1992; Quinlan et al., 1999). Mice were divided into three groups—the normal light/dark cycle group (LR; control), the dark-reared group (DR; animals were placed in the dark for 5 days before visual cortex dissection at P26), and the dark-reared group that was exposed to light 2 h before tissue dissection (DR + LE)—and their visual cortices were analyzed for phospho-GluN2A content in the synaptic plasma membrane (SPM) fraction (Figure 2C). Consistent with a role for this phosphorylation in activity-dependent receptor trafficking and modulation, we detected a significant decrease in the level of phosphorylated GluN2A-S1459 in the DR condition, which was reversed in the DR + LE condition (Figure

2D). These data indicate a dynamic regulation of GluN2A-S1459 phosphorylation *in vivo* by synaptic activity and during development.

The Phosphorylation State of GluN2A-S1459 Modulates PDZ-Binding Domain Interactions

Because the PDZ-binding domain of GluN2A mediates diverse protein-protein interactions, we next assessed whether the phosphorylation of S1459, just 2 residues upstream of the PDZ ligand, could affect GluN2A protein interactions. We evaluated the interaction with the archetypal PDZ-binding domain interactor PSD-95 (Won et al., 2017). We also tested the interaction with the endocytic protein SNX27 because recent findings point to a phosphorylation-dependent enhancement of SNX27 binding to GluN2B (Clairfeuille et al., 2016). Therefore, we tested changes in GluN2A-PSD-95 and GluN2A-SNX27 interactions using both pull-down assays from WT mouse brains and co-immunoprecipitations (coIPs) from HEK293T cells expressing NMDARs and PSD-95 or SNX27. We observed distinct effects of GluN2A-S1459 phosphorylation on PSD-95 and SNX27 binding. Specifically, mimicking the phosphorylation of GluN2A-S1459 decreased the binding to PSD-95 in both pull-down assays (Figures 3A and 3C) and coIPs (Figures 3B and 3C). In sharp contrast, when we analyzed the binding to the endocytic protein SNX27, we observed that the phosphorylation of GluN2A-S1459 enhances this interaction in pull-down assays (Figures 3D and 3F) and coIPs (Figures 3E and 3F). Conversely, using a phospho-dead mutant of this site abolishes the improved interaction. Because SNX27 was previously shown to regulate the surface levels of GluN1 and GluN2B (Clairfeuille et al., 2016; Wang et al., 2013) and phosphorylation of GluN2A-S1459 plays a role in the modulation of the interaction of GluN2A with this protein, we assessed the distribution of the phosphorylated subunit in the SNX27 conditional knockout (cKO) mouse model. We observed that the expression of GluN2A-phosphoS1459 in the PSD fraction of SNX27 cKOs was significantly reduced (Figures 3G and 3H). These results support a model in which GluN2A is phosphorylated in endosomes, which leads to increased interaction with SNX27 and enhanced recycling to the cell surface. Once at the surface, GluN2A-S1459 likely is dephosphorylated, which would promote increased binding to MAGUKs and stabilization at synaptic sites.

Phosphorylation of S1459 Regulates GluN2A Trafficking

Because GluN2A-S1459 phosphorylation affects receptor interactions with SNX27 and PSD-95, we tested whether this PTM regulates NMDAR trafficking. We started by assessing the surface expression of GluN2A phospho mutants in transfected cultured hippocampal neurons, and we observed a significant decrease in the surface levels of the phospho-null GluN2A-S1459A relative to WT (Figures 4A and 4B). Notably, we observed a corresponding change in dendritic spine number, which was decreased in the GluN2A-S1459A-expressing neurons (Figures 4C and 4D) compared to WT and GluN2A-S1459D, suggesting compromised neuronal activity or decreased synapse stability, as a consequence of the reduced surface expression of GluN2A-containing receptors. In addition, this effect is consistent with the possibility that this phosphorylation event may be important during development for the GluN2B-to-GluN2A subunit switch. This hypothesis is supported by the observation that the phosphorylation of this residue peaks before the subunit switch during the first postnatal week in the mouse brain (Figure 2).

Because phosphorylation of GluN2A-S1459 enhances the interaction with the endocytic protein SNX27 and is therefore likely to promote recycling of the receptors to the cell surface, we next evaluated the trafficking of a chimera to specifically measure the endocytic signals within the CTD. To this end, we used the Tac-GluN2A (last 175 amino acids [aa] of the CTD) construct designed to effectively track surface expression, endocytosis, and post-endocytic sorting driven by the GluN2A C-terminus. The protein Tac exhibits robust surface expression, and by appending the C-terminal domains of NMDARs, we can analyze endocytic sorting differences in WT versus mutant chimeric proteins. As expected, these chimeras are strongly targeted to the cell surface and display a highly normalized surface expression (Figure S2), which allows for direct comparisons of post-endocytic differences due to mutations (Lavezzari et al., 2004; Roche et al., 2001; Scott et al., 2001). We measured the co-localization of internalized Tac-GluN2A (WT or mutants) with the recycling endosome marker Rab11 in HeLa cells. We observed that Tac-GluN2A-S1459D co-localization with Rab11 increased over time, whereas that of the phospho-dead mutant did not (Figures 4E and 4F). This indicates that phospho-mimetic GluN2A traffics more efficiently via the recycling endosomal pathway, again pointing to a modulatory role of this phosphorylation event on NMDAR trafficking. Overall, our observations are consistent with a role of GluN2A-S1459 phosphorylation in regulating receptor levels at the surface, with phosphorylation contributing to the receptor targeting to the synaptic membrane.

The Epilepsy-Associated Variant GluN2A-S1459G Impairs NMDAR Interactions, Trafficking, and Excitatory Transmission

Because phosphorylation of GluN2A-S1459 modulates NMDAR interactions and trafficking, it was important to test these parameters using the rare variant GluN2A-S1459G, which may help explain disease etiology. We found a decreased interaction of GluN2A-S1459G with PSD-95 relative to WT in pull downs (Figures 5A and 5C) and coIPs (Figures 5B and 5C). We next assessed the interaction with SNX27, and we also observed the decreased binding of GluN2A-S1459G with SNX27 in both pull-down assays (Figures 5D and 5F) and coIPs (Figures 5E and 5F). These effects indicated that the epilepsy-associated variant of the GluN2A-S1459 phosphorylation site impairs multiple NMDAR interactions that occur via the PDZ-binding domain, leading us to test the effects on receptor surface expression and trafficking.

We next evaluated endocytic sorting of the GluN2A-S1459G variant, which has reduced binding to SNX27. We expressed Tac-GluN2A-S1459G in HeLa cells and assessed the time course of co-localization with Rab11 (Figure 5G). We found no differences in the expression levels of this chimera relative to WT or the phospho mutants (Figure S2); however, in contrast to the phospho-mimetic sorting, we observed that Tac-GluN2A-S1459G had a low level of Rab11 colocalization, which did not increase over time. This change in trafficking may reflect that receptors harboring this mutation are sorted less efficiently to recycling endosomes, resulting in a decreased surface expression of NMDARs. Accordingly, we detected a significant decrease in the neuronal surface expression of GluN2A-S1459G, relative to WT (Figures 5H and 5I). This effect is in accordance with the protein-protein interaction defects we observed. The decreased interaction of the epilepsy-associated variant with SNX27 indicates less efficient trafficking to the synapse, and the defects in PSD-95

binding could destabilize the receptor, even if GluN2A-containing receptors reach the surface membrane. We also found a corresponding decrease in spine density in neurons expressing GluN2A-S1459G (Figures 6A and 6B), which is again consistent with a decrease in neuronal activity as a consequence of impaired GluN2A surface expression.

What consequences do the defect in GluN2A-S1459G trafficking have on excitatory synaptic transmission? To investigate, we measured excitatory synaptic transmission in neurons expressing GluN2A (WT or S1459G). We observed no change in the amplitude of mEPSCs in transfected neurons (Figure 6D), but we did find a significant decrease in mEPSC frequency in neurons expressing the rare variant compared to WT GluN2A (Figures 6C and 6E). This result reveals synaptic defects elicited in neurons expressing this rare variant that are consistent with the spine reduction. Overall, these data reveal impaired GluN2A-containing NMDAR trafficking and subsequent signaling with the epilepsy-associated variant.

DISCUSSION

Epilepsy is a neurological disorder comprising a variety of diagnostic classifications. The most notable clinical manifestation of epilepsy is the occurrence of seizures, with ensuing adverse effects on patients' quality of life, including cognitive, psychological, and social deficits. Epilepsy is estimated to affect 1.2% of the US population, with a higher incidence in younger and older age groups (infancy and older than 60 years of age, respectively) (Devinsky et al., 2018). Recent genomic advances have provided important insights into the genetics of neurodevelopmental disorders such as ASD/ID and epilepsy. Gene Ontology analyses have identified clusters of genes associated with specific cellular functions, including synapse-associated genes (De Rubeis et al., 2014; Sanders et al., 2015; Zoghbi and Bear, 2012). One notable aspect of these disorders is that they share a high degree of comorbidity and converging mechanisms. The *GRIN* genes, which encode the NMDAR subunits, have a prominent role, with *GRIN2B* now considered a high-confidence ASD-associated gene. Although the *GRIN2A* gene is also identified in ASD/ID patients, it is highly associated with epilepsy pathologies, more so than *GRIN2B* (Ogden et al., 2017; XiangWei et al., 2018). Therefore, investigating the role of GluN2A in epilepsy is important and will, it is hoped, reveal mechanisms that can facilitate the development of therapeutics.

In recent years, there have been efforts to functionally characterize pathogenic variants of *GRIN* genes, particularly the ASD/ID-associated *GRIN2B* mutations and the epilepsy/ID-causative *GRIN2A* variants. Most of these studies have focused on variants that result in mutations in residues of the ligand-binding domain, the channel pore, and the linker regions (Table S1), which seem to be the most deleterious, as they are likely to directly affect receptor channel function (Ogden et al., 2017; Swanger et al., 2016). Mutations in the CTD, however, also have damaging potential, since they often have dramatic effects on receptor trafficking and stabilization at the membrane (Liu et al., 2017), and consequently, can have a profound impact on synaptic transmission and plasticity (reviewed by Vieira et al., 2020). The PDZ-binding domain, in particular, exerts a regulatory role in NMDAR trafficking and stabilization due to its ability to interact with a plethora of PSD proteins that contain PDZ domains (Sanz-Clemente et al., 2010, 2013a). A range of functional

consequences have been identified, leading to both hyper- and hypofunction of NMDARs. For GluN2A, the mutations classified as gain of function generally lead to increased agonist potency (e.g., L812M, M817V); decreased sensitivity to channel blockers such as Mg^{2+}, zinc, or protons (e.g., N615K, L812M, M817V); or altered electrophysiological properties of the channel that contribute to increased current amplitude or response time (e.g., P552R, L812M, M817V) (Ogden et al., 2017; Endele et al., 2010; Pierson et al., 2014; Yuan et al., 2014). Conversely, GluN2A loss-of-function mutants generally result in increased sensitivity to negative modulators (e.g., D731N), reduced surface expression (e.g., G483R, R518H), or altered channel properties leading to reduced function (e.g., G483R, R518H, D731N) (Gao et al., 2017; Lesca et al., 2013; Sibarov et al., 2017; Swanger et al., 2016) (Table S1). Studies on the variants affecting the CTD of GluN2 subunits are less common. The present study is, to our knowledge, the first report describing receptor dysfunction elicited by an epilepsy patient mutation in the CTD of GluN2A. Another recent report found altered spine density and reduced surface expression of NMDARs harboring a mutation in the CTD of GluN2B (S1415L) (Liu et al., 2017). It is thus important to expand our knowledge of CTD variants to find common mechanisms of dysfunction that can be pharmacologically targeted. Here, we investigated the functional effects of a rare variant of GluN2A (p.S1459G), identified in a patient presenting with epilepsy and moderate ID (ClinVar; Bowling et al., 2017).

We found that the rare variant *GRIN*2A c.4375A>G, which results in a substitution of GluN2A-S1459 for glycine, contributes to trafficking defects and changes in protein-protein interactions established by the receptor, possibly due to its location, just 2 aa upstream of the PDZ-binding domain of GluN2A, as has been observed for other residues in the vicinity of the PDZ-binding domain of GluN2B (Clairfeuille et al., 2016). We also found decreased spine density and reduction in the frequency of mEPSCs in neurons expressing the GluN2A-S1459G subunit, which reveals a defect in excitatory transmission due to the *de novo* mutation. The reduction of mEPSC frequency in these neurons is likely due to the decrease of spine density, although we cannot exclude the possibility that postsynaptic expression of GluN2A-S1459G may regulate presynaptic glutamate release probability. How the GluN2A-S1459G mutation leads to spine and synaptic transmission deficits remains unknown. It is possible that GluN2A-S1459G exerts a direct modulatory effect on spinogenesis. Alternatively, the GluN2A-S1459G mutation may induce a homeostatic process that indirectly decreases spine development and synaptic transmission (Müller et al., 1993). Nevertheless, the altered trafficking, sorting, and protein interactions of GluN2A-S1459G likely result in the hypofunction of NMDARs harboring this rare variant, which suggests that the phenotype observed in the patient results from reduced GluN2A-containing NMDAR trafficking and signaling. As discussed, while many reports indicate that epilepsy is a consequence of the hyperfunction of NMDARs (Endele et al., 2010; Lemke et al., 2013; Marwick et al., 2019b), which leads to hyper-excitability, our current findings implicate receptor hypofunction, and this has also been observed in other studies (Addis et al., 2017; Strehlow et al., 2019; Swanger et al., 2016). These data demonstrate that changes to normal NMDAR function have deleterious effects. How can NMDAR-impaired function lead to an epilepsy phenotype? While the definitive answer remains elusive, such an effect may be mediated by a differential impact of altered NMDAR subunit expression and function

in distinct types of neurons. GluN1 and GluN2A/B subunit expression is not limited to glutamatergic neurons, but it is present in GABAergic interneurons in the human cortex (Bagasrawala et al., 2017). It is therefore possible that the dysfunction of NMDARs in these classes of neurons could lead to an imbalance in excitatory/inhibitory transmission and, consequently, contribute to epilepsy. It is also plausible that NMDAR hypofunction may increase neuronal excitability (Homayoun and Moghaddam, 2007; Tatard-Leitman et al., 2015), which could contribute to epilepsy. Future experiments investigating the role of the GluN2A-S1459G variant in interneurons and in excitability in pyramidal neurons will shed light onto the mechanisms underlying seizures and epilepsy in patients harboring this variant.

We also identified a role for the phosphorylation of this residue, GluN2A-S1459, in NMDAR trafficking. Many studies have demonstrated that phosphorylation is a highly regulated PTM that contributes to the fine modulation of NMDARs (Roche et al., 2001; Sanz-Clemente et al., 2013a, 2013b). The CTD of NMDAR subunits has many identified phosphorylation sites that affect receptor trafficking and membrane insertion, as well as protein-protein interactions, often dynamically regulated by activity. One of the most prominent kinases in synaptic function is CaMKII, which is not only one of the most abundant proteins at the synapse but has also been found to play paramount roles in synaptic plasticity via mechanisms that are both dependent and independent of its kinase activity (Bayer and Schulman, 2019, Shonesy et al., 2014). In fact, GluN2B is phosphorylated by CaMKIIα following synaptic activity. After NMDAR activation, CaMKIIα is recruited to the PSD, undergoes autophosphorylation (thereby becoming autonomously active), and phosphorylates its synaptic substrates, namely GluN2B and GluA1. The phosphorylation of these subunits exerts modulatory roles on the mechanisms that tightly regulate glutamate receptor trafficking (Bayer and Schulman, 2019) and, consequently, their abundance at the synapse. Even though GluN2B has long been recognized as a CaMKIIα substrate, there was no evidence for direct phosphorylation of the GluN2A subunit by this kinase. We were thus surprised when we found that GluN2A is robustly phosphorylated at S1459, and that this phosphorylation event is mediated by CaMKIIα. Although this phosphorylated residue —GluN2A-S1459—had been identified in phosphoproteomic studies (Goswami et al., 2012; Munton et al., 2007; Trinidad et al., 2006; Tweedie-Cullen et al., 2009), it had not been independently validated, nor had the relevant kinase been found. Here, we demonstrate the endogenous phosphorylation of this residue, but also that it is an activity-regulated and developmentally -regulated event.

The developmental switch of NMDAR subunits is a well-characterized mechanism of synapse maturation that leads to a change in NMDAR properties at the PSD, resulting from the replacement of a predominantly GluN2B-containing population to a GluN2A-rich pool of receptors (Barria and Malinow, 2002; Sheng et al., 1994; Yashiro and Philpot, 2008). In rodents, this subunit shift is known to occur at approximately the second postnatal week and to be facilitated by GluN2B phosphorylation mediated by CK2 (Sanz-Clemente et al., 2010). CK2 is recruited to NMDARs by direct binding to CaMKIIα, thereby forming a trimolecular complex that facilitates the phosphorylation of GluN2B subunits at S1480 within the PDZ-binding domain (Sanz-Clemente et al., 2013a). Phosphorylation of GluN2B-S1480 disrupts the interaction with PSD-95 and promotes endocytosis of NMDARs (Chung

et al., 2004). The present report shows that the phosphorylation of GluN2A at S1459 could also play a role, as we observed a peak of phosphorylation of this residue that precedes the subunit switch, which indicates that it could function as a signal for GluN2A membrane insertion. Phosphorylation of GluN2A-S1459 is proposed here to contribute to increased trafficking of GluN2A-containing receptors to the PSD, namely due to improved binding to the endocytic protein SNX27. Accordingly, we observed altered distribution of the phosphorylated subunit in the SNX27 cKO mouse, which is in accordance with previous reports showing reduced synaptic expression of NMDARs in SNX27 KOs (Loo et al., 2014; Wang et al., 2013). A recent report found that the GluN2B/GluN2A developmental subunit switch occurs independently of the NMDAR subunit CTD (McKay et al., 2018), due to the observation that mice expressing the chimeric GluN2A$^{2B\text{-}CTD}$ undergo a normal subunit shift. The disparity found by McKay et al. (2018) compared to evidence from the current and previous reports, could arise from the fact that SNX27 contributes to the trafficking of both GluN2A-containing receptors, as demonstrated here, and GluN2B-containing receptors (Clairfeuille et al., 2016). As a consequence, even in neurons expressing the chimeric subunits GluN2A$^{2B\text{-}CTD}$ or GluN2B$^{2A\text{-}CTD}$, trafficking of NMDARs that is facilitated by SNX27 could still occur and thus mask putative defects resulting from the altered phosphorylation of GluN2B-S1480 (Sanz-Clemente et al., 2010) or GluN2A-S1459, as well as additional CTD-dependent mechanisms that are not yet resolved.

Consistent with a role of CaMKIIα phosphorylation of GluN2A in NMDAR trafficking, we found that a phospho-null mutant, GluN2A-S1459A, leads to reduced surface expression and that GluN2A is trafficked via the recycling endosomal pathway when this serine is phosphorylated. The proximity of this phosphorylation site to the PDZ-binding domain led us to hypothesize that these trafficking effects are, at least partially, due to the modulation of protein-protein interactions via the PDZ-binding domain of GluN2A, in particular with SNX27 and PSD-95. As discussed, the endocytic protein SNX27 has been shown to contribute to GluN2B-containing NMDAR recycling in a subunit phosphorylation-dependent manner (Clairfeuille et al., 2016). In this report, we extend these findings to the GluN2A subunit, which we show to interact more strongly with SNX27, when the subunit is phosphorylated at S1459. Here, we also find an effect on the binding to PSD-95, which is dramatically decreased upon the phosphorylation of GluN2A; thus, the phosphorylation dictates with which binding protein the NMDAR will associate. These findings suggest that GluN2A is phosphorylated by CaMKIIa when present in endocytic vesicles, which promotes the binding to SNX27. This improved interaction leads to the increased surface delivery of GluN2A-containing receptors, which are likely dephosphorylated to promote the binding to PSD-95, anchoring NMDARs at the synapse. This dramatic modulation of protein-protein interactions affecting receptor trafficking by a single residue phosphorylation resembles α-amino-3-hydroxy-5-methyl-4-isoxazolepropionic acid (AMPA) receptor interactions with proteins interacting with C kinase-1 (PICK1)/glutamate receptor interacting protein 1 (GRIP1). Phosphorylation of the GluA2 subunit at S880, mediated by PKC, modulates PDZ-binding domain interactions, such that when phosphorylated, the GluA2-GRIP1 interaction is disrupted, but the binding to PICK1 is unaffected, leading to receptor internalization (Chung et al., 2000).

Overall, our findings describe several layers of regulation of a single residue of GluN2A, S1459. We wanted to explore the functional consequence of a disease-associated variant, GluN2A-S1459G, because of its provocative location at the extreme CTD of GluN2A. Our studies identified a novel CaMKIIα target within NMDARs, GluN2A-S1459, which is regulated *in vivo* in development and in response to synaptic activity triggered by environmental stimuli. The phosphorylation of GluN2A-S1459 has a robust and inverse effect on binding to two postsynaptic proteins implicated in receptor trafficking and synaptic localization, SNX27 and PSD-95. Notably, our evidence shows that neurons expressing the epilepsy mutant have reduced spine density and reduced mEPSC frequency. While these data cannot be definitively linked to the reduced synaptic expression of GluN2A-S1459G, that possibility is supported by other observations regarding the phosphorylation of GluN2A and the epilepsy mutant. For example, in WT animals, the phosphorylated subunit accumulates in the PSD fraction, and this distribution is affected by conditionally knocking out SNX27, underscoring a role of this phosphorylation event in receptor trafficking. In addition, we observed the reduced surface expression of both the phospho-dead mutant and the S1459G variant, which is consistent with a reduction in synaptic NMDARs, since a large body of literature points to a predominantly synaptic expression of GluN2A-containing receptors (Groc et al., 2006; Liu et al., 2004; Thomas et al., 2006). In fact, recent work using super-resolution microscopy revealed a nanodomain organization of GluN2A- and GluN2B-containing receptors, with a larger number of endogenous GluN2A receptor nanodomains at synaptic versus non-synaptic sites (Kellermayer et al., 2018). In conclusion, our findings demonstrate the importance of studies on human variants in understanding NMDAR function and have the potential to elucidate links between receptor trafficking defects and disease etiology.

STAR★METHODS

RESOURCE AVAILABILITY

Lead Contact—Further information and requests for resources and reagents should be directed to, and will be fulfilled by the Lead Contact, Katherine

W. Roche (rochek@nih.gov).

Materials Availability—All unique reagents generated in this study are available from the Lead Contact with a completed Materials Transfer Agreement.

Data and Code Availability—This study did not generate datasets/code.

EXPERIMENTAL MODEL AND SUBJECT DETAILS

Animals—The NINDS Animal Care and Use Committee approved all procedures and animal use (protocol #1171). Male and female C57BL/6 inbred mice (Charles River) were used at P7–2 months old, for brain fractionation experiments. Mice were housed on a standard 12 h dark and light cycle. For dark rearing experiments, male and female C57BL/6J littermates were housed in a normal light/dark cycle (12h light, 12h dark) from P0 to P26 (light reared, LR). Alternatively, mice were relocated to complete darkness from P21 to

P26 (dark reared, DR), or kept in complete darkness from P21 to P26, but exposed to 2h of light before tissue was harvested (DR plus light exposure, DR+LE). The primary visual cortex was dissected in the dark for the DR condition or in the light for the LR and DR+LE conditions. Synaptic plasma membrane (SPM) fractions were prepared.

We developed the SNX27 cKO by backcrossing the mouse strains Snx27$^{tm1a(KOMP)Wtsi}$ and B6;SJL-Tg(ACTFLPe)9205Dym/J, followed by backcrossing of the Flp-SNX27 homozygous animals (F3) with FVB/N-Tg(Thy1-cre)1Vln/J mice, to delete expression of SNX27 in the postnatal cortex and hippocampus. Mouse CRE negative littermates of either sex were used as controls for the mouse SNX27 cKO brain fractionation experiments.

Neuronal cultures—Primary cultures of hippocampal neurons were prepared from male and female E18 Sprague-Dawley rats (Envigo) as previously described (Roche and Huganir, 1995), and following the NIH Guide for the Care and Use of Laboratory Animals. In brief, the pregnant females were narcotized with CO_2 and the embryos removed. The brains were removed, hippocampi dissected, and neurons dissociated before being plated in poly-D-lysine (Sigma, P7280) coated coverslips. For imaging experiments, hippocampal neurons were plated on 12 well dishes at 100,000 cells/well; for electrophysiology experiments, hippocampal neurons were plated on 24 well dishes at 200,000 cells/well. The mixed gender cultures were maintained in Neurobasal medium (Life Technologies, Cat#21103–049) supplemented with 2% B27 (Life Technologies, Cat#17504–044) and 2 mM L-glutamine (Sigma-Aldrich, Cat#G-7513) at 37°C and 5% CO_2 for 17 days. At DIV 13 neurons were transfected using Lipofectamine 2000 (Invitrogen, 11668–019) with 2.5 μg GFP-GluN2A constructs (plus 0.5 μg pCAG-GFP for spine density analysis and electrophysiology experiments).

Cell lines—HEK293T and HeLa cell lines were used (ATCC). Briefly, cells were maintained in DMEM (GIBCO, 11966025) supplemented with 10% fetal bovine serum (FBS) (Hyclone, SH30071.03) and 1% glutamine (GIBCO, 25030081), at 37°C and 5% CO_2. HEK293T were cultured in 6 cm dishes and transfected one day after plating using Lipofectamine 2000 as previously described (Won et al., 2016). We co-expressed GFP-GluN2A (WT or mutants, as indicated), GluN1 and CaMKIIα (WT, K42R or T286D, as annotated) (ratio 2:1:1). Cells were maintained in 20 mM $MgCl_2$ to avoid excitotoxicity. Two days after transfection, HEK293T cells were harvested in cold PBS, centrifuged at 15,000xg for 20 min and resuspended in Tris buffer (pH 7.5) containing 1% SDS, sonicated and incubated for 30 min, at 37°C. Sample buffer was then added to the lysates and proteins denatured at 42°C for 20 min. The samples were then analyzed using immunoblotting. HeLa cells were cultured on glass coverslips, in duplicate, and transfected with Tac-GluN2A chimeras (0.5 mg/coverslip) and GFP-Rab11 (0.5 mg/coverslip).

METHOD DETAILS

DNA constructs and antibodies—Site-directed mutagenesis was performed on the pRK5-GFP-GluN2A, pGEX4-GST-GluN2A CTD (corresponding to the last 175 aa of GluN2A) or pRK5-Tac-GluN2A (last 175 aa) to obtain the S1459A; S1459D; and S1459G mutants.

***In vitro* kinase assays—**Purified GST-fusion proteins (GST; GST-GluN2A WT or GST-GluN2A-S1459A) were subjected to *in vitro* phosphorylation with PKA, PKC or CaMKIIα to identify the kinase(s) responsible for GluN2A-S1459 phosphorylation. For PKA phosphorylation, the fusion proteins were incubated in 10 mM 4-(2-hydroxyethyl)-1-piperazineethanesulfonic acid (HEPES; pH 7.0), 20 mM $MgCl_2$, 50 μM ATP and 1 pmol of [$\gamma-^{32}$P]-ATP (3,000 Ci mmol^{-1}) with 50 ng of purified PKA catalytic subunit (Promega). For PKC phosphorylation, reactions were performed in 20 mM HEPES, pH 7.4, 1.67 mM $CaCl_2$, 1 mM DTT, 10 mM $MgCl_2$, 50 μM ATP and 1 pmol of [$\gamma-^{32}$P]-ATP (3,000 Ci mmol^{-1}) with 10 ng of purified PKC (Promega). For CaMKIIα phosphorylation, reactions were in 20 mM Tris-HCl (pH 7.5), 10 mM $MgCl_2$, 0.5 mM DTT, 0.1 mM EDTA, 2.4 μM calmodulin, 2 mM $CaCl_2$, 100 μM ATP and 1 pmol of [$\gamma-^{32}$P]ATP (3,000 Ci mmol^{-1}) with 25 ng of recombinant CaMKIIα (Calbiochem). All *in vitro* kinase assays were performed at 30°C for 30 min. The reactions were stopped with addition of SDS-PAGE sample buffer and incubation at 42°C for 20 min. The proteins were resolved by SDS-PAGE and visualized by autoradiography. Alternatively, SDS-PAGE–resolved proteins were transferred to nitrocellulose membranes and assayed for phosphorylation by immunoblotting with GluN2A-phosphoS1459 antibody. Total protein was assessed by staining the gels with Coomassie Brilliant Blue (CBB, Expedeon).

Subcellular fractionation of mouse brain—Mouse WT or SNX27 cKO brains (2–3 months old adults, both sexes; or at the indicated ages) were fractionated as previously described (Hallett et al., 2008). The brains were homogenized in ice-cold TES buffer [320 mM sucrose, 10 mM Tris·HCl (pH 7.5), 5 mM EDTA, 1 × protease inhibitor mixture, and phosphatase inhibitor mixtures II and III]. Homogenates (H) were centrifuged at 1,000 × g for 10 min at 4°C. The supernatant (S1) was centrifuged at 10,000 × g for 15 min at 4°C to obtain the crude synaptosomal membrane fraction (P2). The P2 pellet was resuspended in ice-cold TES buffer (35.6 mM sucrose, 10 mM Tris·HCl pH 7.5, 5 mM EDTA, 1 × protease inhibitor mixture, and phosphatase inhibitor mixtures II and III) and was incubated on ice for 30 min followed by centrifugation at 25,000 × g for 20 min at 4°C to obtain the SPM. The pellet was resuspended in 1% Triton X-100 buffer [10 mM Tris·HCl (pH 7.5), 5 mM EDTA, 1 × protease inhibitor mixture, and phosphatase inhibitor mixture II and III] and incubated with gentle agitation at 4°C for 30 min. Lysates were centrifuged at 33,000 × g for 30 min at 4°C to obtain the soluble fraction (Triton X-100–soluble) and the Triton X-100–insoluble/PSD fraction (pellet), which was solubilized by brief sonication and heating at 37°C for 30 min in 1% SDS [10 mM Tris·HCl (pH 7.5), 5 mM EDTA, 1 × protease inhibitor mixture, and phosphatase inhibitor mixtures II and III]. To obtain the PSD fraction, the lysates were centrifuged at 100,000 × g for 20 min at 4°C. After obtaining the PSD fraction from WT brains, 20 μg of protein from the PSD were incubated with or without lambda phosphatase (New England Biolabs) at 37°C, for 1h, to assess antibody specificity.

Immunofluorescence microscopy—NMDAR trafficking was analyzed using immunocytochemistry. We expressed GFP-tagged GluN2A (WT or mutants) in DIV13 rat hippocampal neurons, using Lipofectamine 2000 transfection. At DIV17, we analyzed receptor surface expression or spine density, as previously described (Liu et al., 2017; Sanz-

Clemente et al., 2013a; Suh et al., 2010). Briefly, we stained surface GFP-tagged GluN2A using rabbit GFP antibody for 15 min, at RT, followed by 3 washes with PBS. For analysis of surface expression, we immediately fixed the cells with 4% PFA, for 7 min, at RT and then labeled with Alexa fluor 488-conjugated secondary antibody. After permeabilization, the intracellular pool of receptors was stained using a chicken GFP antibody followed by labeling with Alexa fluor 555 secondary antibody.

To analyze spine density, we co-transfected pCAG-GFP with the GluN2A constructs and then, at DIV 17, we fixed the cells and mounted the coverslips. All immunofluorescence imaging was carried out in a Zeiss LSM800 confocal microscope and serial optical sections collected at 0.35 mm intervals were used to create maximum projection images. Quantification was performed by analyzing the fluorescence intensity of 3 independent areas per neuron (secondary or tertiary dendrites) using MetaMorph 6.0 software and is presented as ratios of intensity (mean ± SEM) or as the number of spines/dendritic area.

Tac-GluN2A chimera endocytosis assay—To assess the influence of S1459 on the endocytic sorting of GluN2A, we induced internalization of Tac-GluN2A constructs in HeLa cells, as previously described (Lavezzari et al., 2004), with minor modifications. These chimeras consist of the last 175 aa of the GluN2A CTD (WT or mutants) appended to the Tac protein, which is a stable surface integral membrane protein. As such, the chimeras are almost exclusively expressed at the cell surface (Lavezzari et al., 2004), which allows the assessment of the impact of point mutations in the GluN2A CTD on receptor internalization. One day after co-transfection with Tac-GluN2A constructs and GFP-Rab11, HeLa cells were incubated with anti-Tac antibody on ice for 1h. The cells were then returned to 37°C for the indicated periods of time (5, 15 or 30 min) to allow Tac internalization. The cells were wfigureashed and fixed in 4% PFA in PBS for 15 min at RT and surface Tac labeled with Alexa fluor 555 antibody. HeLa cells were then permeabilized and blocked with 10% NGS. Internalized Tac and GFP-Rab-11 were then labeled with Alexa fluor 633 or 488 secondary antibodies, respectively. Finally, the coverslips were washed again and mounted on glass slides. Analysis of internalized Tac and GFP-Rab11 colocalization was performed using a Zeiss LSM800 confocal microscope and the ImageJ software (JaCOP plugin) and presented as the fraction of internalized Tac co-localizing with GFP.

Co-immunoprecipitation (co-IP) and pull-down assays—For pull-down assays from mouse brain, we incubated GST-GluN2A C-terminal domains (aa 1289–1464; pre-blocked with 3% NGS in PBS) with total homogenate (for SNX27 binding) or P2 fractions (for PSD-95 interaction) from WT animals (solubilized with 1% SDS buffer and neutralized with 1% Tx-100 buffer). The samples were incubated at 4°C for 2h and then washed 3 times with 1% Triton X-100 buffer. Samples were resolved in two sister gels, one used for analysis of interacting partners and the other for comparison of GST protein loading using CBB staining.

For co-IP assays, HEK293T cells were transfected with GFP-GluN2A (WT or mutants, as indicated), GluN1 and either Myc-PSD-95 (ratio 10:5:1) or Myc-SNX27 (ratio 2:1:1), as appropriate. Cells were maintained in 20 mM $MgCl_2$ to avoid excitotoxicity. Two days after transfection, HEK293T cells were harvested in cold PBS, centrifuged at 15,000 x g

for 20 min and resuspended in Tris buffer (pH 8.8) containing 1% DOC, sonicated and incubated for 30 min, at 37°C (Won et al., 2016). The lysates were then neutralized with Tris pH 7.5 with 1% Triton X-100, at 4°C for another 30 min, followed by centrifugation. The supernatant was incubated with 1 μg of GFP antibody, o.n. at 4°C and protein-A beads added to the samples. After 4h incubation at 4°C, the beads were washed 3 times with 1% Triton X-100 buffer. The samples were then resolved in SDS-PAGE and analyzed by immunoblotting, using the appropriate antibodies.

Electrophysiological measurements—Cultured rat hippocampal neurons were co-transfected at DIV 13 with pCAG-GFP and GluN2A WT or S1459G. Whole-cell voltage clamp recordings of mEPSCs were performed in DIV 17–18 cultured rat hippocampal neurons at 20–25°C using glass patch electrodes filled with an internal solution consisting of 135 mM $CsMeSO_4$, 8 mM NaCl, 10 mM HEPES, 0.3 mM Na-GTP, 4 mM Mg-ATP, 0.3 mM EGTA, 5 mM QX-314, and 0.1 mM spermine. The external solutions contained 119 mM NaCl, 2.5 mM KCl, 26 mM $NaHCO_3$, 1 mM Na_2PO_4, 11 mM glucose, 2.5 mM $CaCl_2$, and 1.3 mM $MgCl_2$; 0.1 mM Picrotoxin and 0.5 μM TTX were added to the external solutions before recording. Transfected cells were visualized with fluorescence, and mEPSCs were measured at −70 mV. Series resistance was monitored and not compensated, and cells in which series resistance was more than 25 MΩ or varied by 25% during a recording session were discarded. Synaptic responses were collected with a Multiclamp 700B amplifier (Axon Instruments), filtered at 2 kHz, and digitized at 10 kHz. The analysis of the mEPSCs was done offline semiautomatically, using in-house software in Igor Pro (Wavemetrics) developed in Dr. Roger Nicoll's laboratory at University of California, San Francisco (UCSF).

QUANTIFICATION AND STATISTICAL ANALYSIS

Quantification and analysis of immunoblots and electrophysiology—Immunoblots were analyzed with Image-J by calculating the area under the curve. Intensity was normalized to total GluN2A or tubulin, as indicated in the figure legends; values were then normalized to the control (WT). Statistical analysis was done using Student's t test or one-way ANOVA followed by the appropriate post hoc analysis (Sidak's or Dunnett's multiple comparison tests), as indicated in the figure legends. For electrophysiology, Student's t test was used to calculate statistical significance.

Quantification and analysis of immunocytochemistry—For surface expression of GluN2A in neurons, three dendritic regions were randomly selected per cell. The conditions were blinded to the experimenter during image acquisition and quantification. Metamorph was used to measure surface and intracellular intensity. Analysis was done using one-way ANOVA followed by Sidak's or Dunnett's multiple comparison tests, as indicated. For HeLa cell imaging, Metamorph was used to measure surface and intracellular intensity level of Tac proteins. Analysis was done using one-way ANOVA with Dunnett's multiple comparisons test. For colocalization of Tac and Rab11, Manders' coefficients were calculated using the JACoP plugin in Image-J. Analysis was done using two-way ANOVA with Dunnett's or Tukey's multiple comparisons tests, as indicated.

Statistical analysis

The GraphPad Prism8 software was used for statistical analysis of the data. One-way ANOVA was performed, followed by the appropriate post hoc analysis. Alternatively, Student's t tests were used, when comparing between two groups. For all assays, 3–5 independent experiments were done. Each *n* corresponds to one animal or one independent cell culture. Statistical significance was established for $p < 0.05$. All data are presented as means ± SEM.

Supplementary Material

Refer to Web version on PubMed Central for supplementary material.

ACKNOWLEDGMENTS

We are grateful to Carolyn Smith and the NINDS imaging facility for their assistance. Research was supported by the NINDS Intramural Research Program (to M.M.V., T.A.N., K.W., W.L., J.D.B., and K.W.R.), the Portuguese Foundation for Science and Technology (FCT [Fundação para a Ciência e a Tecnologia]; grant SFRH/BI/106010/2015, to M.M.V.), and the Australian Research Council Discovery Project grant (DP190101390, to V.A. and B.M.C.). B.M.C. is supported by a Senior Research Fellowship from the Australian National Health and Medical Research Council (NHMRC; APP1136021).

REFERENCES

Addis L, Virdee JK, Vidler LR, Collier DA, Pal DK, and Ursu D. (2017). Epilepsy-associated GRIN2A mutations reduce NMDA receptor trafficking and agonist potency - molecular profiling and functional rescue. Sci. Rep 7, 66. [PubMed: 28242877]

Al-Hallaq RA, Conrads TP, Veenstra TD, and Wenthold RJ (2007). NMDA di-heteromeric receptor populations and associated proteins in rat hippocampus. J. Neurosci 27, 8334–8343. [PubMed: 17670980]

Bagasrawala I, Memi F, Radonjic NV, and Zecevic N. (2017). N-Methyl d-Aspartate Receptor Expression Patterns in the Human Fetal Cerebral Cortex. Cereb. Cortex 27, 5041–5053. [PubMed: 27664962]

Barria A, and Malinow R. (2002). Subunit-specific NMDA receptor trafficking to synapses. Neuron 35, 345–353. [PubMed: 12160751]

Barria A, and Malinow R. (2005). NMDA receptor subunit composition controls synaptic plasticity by regulating binding to CaMKII. Neuron 48, 289–301. [PubMed: 16242409]

Bayer KU, and Schulman H. (2019). CaM Kinase: Still Inspiring at 40. Neuron 103, 380–394. [PubMed: 31394063]

Bellone C, and Nicoll RA (2007). Rapid bidirectional switching of synaptic NMDA receptors. Neuron 55, 779–785. [PubMed: 17785184]

Bowling KM, Thompson ML, Amaral MD, Finnila CR, Hiatt SM, Engel KL, Cochran JN, Brothers KB, East KM, Gray DE, et al. (2017). Genomic diagnosis for children with intellectual disability and/or developmental delay. Genome Med. 9, 43. [PubMed: 28554332]

Carmignoto G, and Vicini S. (1992). Activity-dependent decrease in NMDA receptor responses during development of the visual cortex. Science 258, 1007–1011. [PubMed: 1279803]

Carvill GL, Regan BM, Yendle SC, O'Roak BJ, Lozovaya N, Bruneau N, Burnashev N, Khan A, Cook J, Geraghty E, et al. (2013). GRIN2A mutations cause epilepsy-aphasia spectrum disorders. Nat. Genet 45, 1073–1076. [PubMed: 23933818]

Chung HJ, Xia J, Scannevin RH, Zhang X, and Huganir RL (2000). Phosphorylation of the AMPA receptor subunit GluR2 differentially regulates its interaction with PDZ domain-containing proteins. J. Neurosci 20, 7258–7267. [PubMed: 11007883]

Chung HJ, Huang YH, Lau LF, and Huganir RL (2004). Regulation of the NMDA receptor complex and trafficking by activity-dependent phosphorylation of the NR2B subunit PDZ ligand. J. Neurosci 24, 10248–10259. [PubMed: 15537897]

Clairfeuille T, Mas C, Chan AS, Yang Z, Tello-Lafoz M, Chandra M, Widagdo J, Kerr MC, Paul B, Mé rida I, et al. (2016). A molecular code for endosomal recycling of phosphorylated cargos by the SNX27-retromer complex. Nat. Struct. Mol. Biol 23, 921–932. [PubMed: 27595347]

Cohen NA, Brenman JE, Snyder SH, and Bredt DS (1996). Binding of the inward rectifier K+ channel Kir 2.3 to PSD-95 is regulated by protein kinase A phosphorylation. Neuron 17, 759–767. [PubMed: 8893032]

Cull-Candy SG, and Leszkiewicz DN (2004). Role of distinct NMDA receptor subtypes at central synapses. Sci. STKE 2004, re16.

Cullen PJ (2008). Endosomal sorting and signalling: an emerging role for sorting nexins. Nat. Rev. Mol. Cell Biol. 9, 574–582. [PubMed: 18523436]

De Rubeis S, He X, Goldberg AP, Poultney CS, Samocha K, Cicek AE, Kou Y, Liu L, Fromer M, Walker S, et al. (2014). Synaptic, transcriptional and chromatin genes disrupted in autism. Nature 515, 209–215. [PubMed: 25363760]

Devinsky O, Vezzani A, O'Brien TJ, Jette N, Scheffer IE, de Curtis M, and Perucca P. (2018). Epilepsy. Nat. Rev. Dis. Primers 4, 18024. [PubMed: 29722352]

Endele S, Rosenberger G, Geider K, Popp B, Tamer C, Stefanova I, Milh M, Kortu€m F, Fritsch A, Pientka FK, et al. (2010). Mutations in GRIN2A and GRIN2B encoding regulatory subunits of NMDA receptors cause variable neurodevelopmental phenotypes. Nat. Genet 42, 1021–1026. [PubMed: 20890276]

Gao K, Tankovic A, Zhang Y, Kusumoto H, Zhang J, Chen W, Xiang-Wei W, Shaulsky GH, Hu C, Traynelis SF, et al. (2017). A de novo loss-of-function GRIN2A mutation associated with childhood focal epilepsy and acquired epileptic aphasia. PLOS ONE 12, e0170818.

Gilman SR, Iossifov I, Levy D, Ronemus M, Wigler M, and Vitkup D. (2011). Rare de novo variants associated with autism implicate a large functional network of genes involved in formation and function of synapses. Neuron 70, 898–907. [PubMed: 21658583]

Goswami T, Li X, Smith AM, Luderowski EM, Vincent JJ, Rush J, and Ballif BA (2012). Comparative phosphoproteomic analysis of neonatal and adult murine brain. Proteomics 12, 2185–2189. [PubMed: 22807455]

Groc L, Heine M, Cognet L, Brickley K, Stephenson FA, Lounis B, and Choquet D. (2004). Differential activity-dependent regulation of the lateral mobilities of AMPA and NMDA receptors. Nat. Neurosci 7, 695–696. [PubMed: 15208630]

Groc L, Heine M, Cousins SL, Stephenson FA, Lounis B, Cognet L, and Choquet D. (2006). NMDA receptor surface mobility depends on NR2A-2B subunits. Proc. Natl. Acad. Sci. USA 103, 18769–18774. [PubMed: 17124177]

Hallett PJ, Collins TL, Standaert DG, and Dunah AW (2008). Biochemical fractionation of brain tissue for studies of receptor distribution and trafficking. Curr. Protoc. Neurosci Chapter 1, Unit 1.16.

Hansen KB, Ogden KK, Yuan H, and Traynelis SF (2014). Distinct functional and pharmacological properties of Triheteromeric GluN1/GluN2A/ GluN2B NMDA receptors. Neuron 81, 1084–1096. [PubMed: 24607230]

Hestrin S. (1992). Developmental regulation of NMDA receptor-mediated synaptic currents at a central synapse. Nature 357, 686–689. [PubMed: 1377360]

Homayoun H, and Moghaddam B. (2007). NMDA receptor hypofunction produces opposite effects on prefrontal cortex interneurons and pyramidal neurons. J. Neurosci 27, 11496–11500. [PubMed: 17959792]

Incontro S, Díaz-Alonso J, Iafrati J, Vieira M, Asensio CS, Sohal VS, Roche KW, Bender KJ, and Nicoll RA (2018). The CaMKII/NMDA receptor complex controls hippocampal synaptic transmission by kinase-dependent and independent mechanisms. Nat. Commun 9, 2069. [PubMed: 29802289]

Jeong J, Pandey S, Li Y, Badger JD 2nd, Lu W, and Roche KW (2019). PSD-95 binding dynamically regulates NLGN1 trafficking and function. Proc. Natl. Acad. Sci. USA 116, 12035–12044. [PubMed: 31138690]

Kellermayer B, Ferreira JS, Dupuis J, Levet F, Grillo-Bosch D, Bard L, Linares-Loyez J, Bouchet D, Choquet D, Rusakov DA, et al. (2018). Differential Nanoscale Topography and Functional Role of GluN2-NMDA Receptor Subtypes at Glutamatergic Synapses. Neuron 100, 106–119.e7. [PubMed: 30269991]

Lavezzari G, McCallum J, Dewey CM, and Roche KW (2004). Subunit-specific regulation of NMDA receptor endocytosis. J. Neurosci 24, 6383–6391. [PubMed: 15254094]

Lemke JR, Lal D, Reinthaler EM, Steiner I, Nothnagel M, Alber M, Geider K, Laube B, Schwake M, Finsterwalder K, et al. (2013). Mutations in GRIN2A cause idiopathic focal epilepsy with rolandic spikes. Nat. Genet 45, 1067–1072. [PubMed: 23933819]

Lesca G, Rudolf G, Bruneau N, Lozovaya N, Labalme A, Boutry-Kryza N, Salmi M, Tsintsadze T, Addis L, Motte J, et al. (2013). GRIN2A mutations in acquired epileptic aphasia and related childhood focal epilepsies and encephalopathies with speech and language dysfunction. Nat. Genet 45, 1061–1066. [PubMed: 23933820]

Lesca G, Møller RS, Rudolf G, Hirsch E, Hjalgrim H, and Szepetowski P. (2019). Update on the genetics of the epilepsy-aphasia spectrum and role of GRIN2A mutations. Epileptic Disord. 21 (S1), 41–47. [PubMed: 31149903]

Liu XB, Murray KD, and Jones EG (2004). Switching of NMDA receptor 2A and 2B subunits at thalamic and cortical synapses during early postnatal development. J. Neurosci 24, 8885–8895. [PubMed: 15470155]

Liu S, Zhou L, Yuan H, Vieira M, Sanz-Clemente A, Badger JD 2nd, Lu W, Traynelis SF, and Roche KW(2017). A Rare Variant Identified Within the GluN2B C-Terminus in a Patient with Autism Affects NMDA Receptor Surface Expression and Spine Density. J. Neurosci 37, 4093–4102. [PubMed: 28283559]

Loo LS, Tang N, Al-Haddawi M, Dawe GS, and Hong W. (2014). A role for sorting nexin 27 in AMPA receptor trafficking. Nat. Commun 5, 3176. [PubMed: 24458027]

Marwick KFM, Skehel PA, Hardingham GE, and Wyllie DJA (2019b). The human NMDA receptor GluN2AN615K variant influences channel blocker potency. Pharmacol. Res. Perspect 7, e00495.

McKay S, Ryan TJ, McQueen J, Indersmitten T, Marwick KFM, Hasel P, Kopanitsa MV, Baxter PS, Martel MA, Kind PC, et al. (2018). The Developmental Shift of NMDA Receptor Composition Proceeds Independently of GluN2 Subunit-Specific GluN2 C-Terminal Sequences. Cell Rep. 25, 841–851.e4. [PubMed: 30355491]

Monyer H, Burnashev N, Laurie DJ, Sakmann B, and Seeburg PH (1994). Developmental and regional expression in the rat brain and functional properties of four NMDA receptors. Neuron 12, 529–540. [PubMed: 7512349]

Müller M, Gähwiler BH, Rietschin L, and Thompson SM (1993). Reversible loss of dendritic spines and altered excitability after chronic epilepsy in hippocampal slice cultures. Proc. Natl. Acad. Sci. USA 90, 257–261. [PubMed: 8093558]

Munton RP, Tweedie-Cullen R, Livingstone-Zatchej M, Weinandy F, Waidelich M, Longo D, Gehrig P, Potthast F, Rutishauser D, Gerrits B, et al. (2007). Qualitative and quantitative analyses of protein phosphorylation in naive and stimulated mouse synaptosomal preparations. Mol. Cell. Proteomics 6, 283–293. [PubMed: 17114649]

Myers KA, and Scheffer IE (2016). GRIN2A-Related Speech Disorders and Epilepsy. In GeneReviews, Adam MP, Ardinger HH, Pagon RA, Wallace SE, Bean LJH, Stephens K, and Amemiya A, eds. (University of Washington, Seattle).

Myers SJ, Yuan H, Kang JQ, Tan FCK, Traynelis SF, and Low CM (2019). Distinct roles of GRIN2A and GRIN2B variants in neurological conditions. F1000Res. 8, F1000 Faculty Rev-1940.

Ogden KK, Chen W, Swanger SA, McDaniel MJ, Fan LZ, Hu C, Tankovic A, Kusumoto H, Kosobucki GJ, Schulien AJ, et al. (2017). Molecular Mechanism of Disease-Associated Mutations in the Pre-M1 Helix of NMDA Receptors and Potential Rescue Pharmacology. PLOS Genet. 13, e1006536.

Pierson TM, Yuan H, Marsh ED, Fuentes-Fajardo K, Adams DR, Markello T, Golas G, Simeonov DR, Holloman C, Tankovic A, et al. ; PhD for the NISC Comparative Sequencing Program (2014). GRIN2A mutation and early-onset epileptic encephalopathy: personalized therapy with memantine. Ann. Clin. Transl. Neurol 1, 190–198. [PubMed: 24839611]

Platzer K, and Lemke JR (2018). GRIN2B-Related Neurodevelopmental Disorder. In GeneReviews, Adam MP, Ardinger HH, Pagon RA, Wallace SE, Bean LJH, Stephens K, and Amemiya A, eds. (University of Washington, Seattle).

Quinlan EM, Olstein DH, and Bear MF (1999). Bidirectional, experience-dependent regulation of N-methyl-D-aspartate receptor subunit composition in the rat visual cortex during postnatal development. Proc. Natl. Acad. Sci. USA 96, 12876–12880. [PubMed: 10536016]

Roche KW, and Huganir RL (1995). Synaptic expression of the high-affinity kainate receptor subunit KA2 in hippocampal cultures. Neuroscience 69, 383–393. [PubMed: 8552236]

Roche KW, Standley S, McCallum J, Dune Ly C, Ehlers MD, and Wenthold RJ (2001). Molecular determinants of NMDA receptor internalization. Nat. Neurosci 4, 794–802. [PubMed: 11477425]

Ryan TJ, Kopanitsa MV, Indersmitten T, Nithianantharajah J, Afinowi NO, Pettit C, Stanford LE, Sprengel R, Saksida LM, Bussey TJ, et al. (2013). Evolution of GluN2A/B cytoplasmic domains diversified vertebrate synaptic plasticity and behavior. Nat. Neurosci 16, 25–32. [PubMed: 23201971]

Sanders SJ, He X, Willsey AJ, Ercan-Sencicek AG, Samocha KE, Cicek AE, Murtha MT, Bal VH, Bishop SL, Dong S, et al. ; Autism Sequencing Consortium (2015). Insights into Autism Spectrum Disorder Genomic Architecture and Biology from 71 Risk Loci. Neuron 87, 1215–1233. [PubMed: 26402605]

Sanhueza M, Fernandez-Villalobos G, Stein IS, Kasumova G, Zhang P, Bayer KU, Otmakhov N, Hell JW, and Lisman J. (2011). Role of the CaMKII/NMDA receptor complex in the maintenance of synaptic strength. J. Neurosci 31, 9170–9178. [PubMed: 21697368]

Sanz-Clemente A, Matta JA, Isaac JT, and Roche KW (2010). Casein kinase 2 regulates the NR2 subunit composition of synaptic NMDA receptors. Neuron 67, 984–996. [PubMed: 20869595]

Sanz-Clemente A, Gray JA, Ogilvie KA, Nicoll RA, and Roche KW (2013a). Activated CaMKII couples GluN2B and casein kinase 2 to control synaptic NMDA receptors. Cell Rep. 3, 607–614. [PubMed: 23478024]

Sanz-Clemente A, Nicoll RA, and Roche KW (2013b). Diversity in NMDA receptor composition: many regulators, many consequences. Neuroscientist 19, 62–75. [PubMed: 22343826]

Satterstrom FK, Kosmicki JA, Wang J, Breen MS, De Rubeis S, An JY, Peng M, Collins R, Grove J, Klei L, et al. (2020). Large-Scale Exome Sequencing Study Implicates Both Developmental and Functional Changes in the Neurobiology of Autism. Cell 180, 568–584.e23. [PubMed: 31981491]

Scott DB, Blanpied TA, Swanson GT, Zhang C, and Ehlers MD (2001). An NMDA receptor ER retention signal regulated by phosphorylation and alternative splicing. J. Neurosci 21, 3063–3072. [PubMed: 11312291]

Sheng M, Cummings J, Roldan LA, Jan YN, and Jan LY (1994). Changing subunit composition of heteromeric NMDA receptors during development of rat cortex. Nature 368, 144–147. [PubMed: 8139656]

Shonesy BC, Jalan-Sakrikar N, Cavener VS, and Colbran RJ (2014). CaMKII: a molecular substrate for synaptic plasticity and memory. Prog. Mol. Biol. Transl. Sci 122, 61–87. [PubMed: 24484698]

Sibarov DA, Bruneau N, Antonov SM, Szepetowski P, Burnashev N, and Giniatullin R. (2017). Functional Properties of Human NMDA Receptors Associated with Epilepsy-Related Mutations of GluN2A Subunit. Front. Cell. Neurosci 11, 155. [PubMed: 28611597]

Strehlow V, Heyne HO, Vlaskamp DRM, Marwick KFM, Rudolf G, de Bellescize J, Biskup S, Brilstra EH, Brouwer OF, Callenbach PMC, et al. ; GRIN2A Study Group (2019). GRIN2A-related disorders: genotype and functional consequence predict phenotype. Brain 142, 80–92. [PubMed: 30544257]

Suh YH, Terashima A, Petralia RS, Wenthold RJ, Isaac JT, Roche KW, and Roche PA (2010). A neuronal role for SNAP-23 in postsynaptic glutamate receptor trafficking. Nat. Neurosci 13, 338–343. [PubMed: 20118925]

Swanger SA, Chen W, Wells G, Burger PB, Tankovic A, Bhattacharya S, Strong KL, Hu C, Kusumoto H, Zhang J, et al. (2016). Mechanistic Insight into NMDA Receptor Dysregulation by Rare Variants in the GluN2A and GluN2B Agonist Binding Domains. Am. J. Hum. Genet 99, 1261–1280. [PubMed: 27839871]

Tarabeux J, Kebir O, Gauthier J, Hamdan FF, Xiong L, Piton A, Spiegelman D, Henrion É ., Millet B, Fathalli F, et al. ; S2D team (2011). Rare mutations in N-methyl-D-aspartate glutamate receptors in autism spectrum disorders and schizophrenia. Transl. Psychiatry 1, e55. [PubMed: 22833210]

Tatard-Leitman VM, Jutzeler CR, Suh J, Saunders JA, Billingslea EN, Morita S, White R, Featherstone RE, Ray R, Ortinski PI, et al. (2015). Pyramidal cell selective ablation of N-methyl-D-aspartate receptor 1 causes increase in cellular and network excitability. Biol. Psychiatry 77, 556–568. [PubMed: 25156700]

Thomas CG, Miller AJ, and Westbrook GL (2006). Synaptic and extrasynaptic NMDA receptor NR2 subunits in cultured hippocampal neurons. J. Neurophysiol 95, 1727–1734. [PubMed: 16319212]

Tovar KR, and Westbrook GL (2002). Mobile NMDA receptors at hippocampal synapses. Neuron 34, 255–264. [PubMed: 11970867]

Trinidad JC, Specht CG, Thalhammer A, Schoepfer R, and Burlingame AL (2006). Comprehensive identification of phosphorylation sites in postsynaptic density preparations. Mol. Cell. Proteomics 5, 914–922. [PubMed: 16452087]

Tweedie-Cullen RY, Reck JM, and Mansuy IM (2009). Comprehensive mapping of post-translational modifications on synaptic, nuclear, and histone proteins in the adult mouse brain. J. Proteome Res. 8, 4966–4982. [PubMed: 19737024]

Vieira M, Yong XLH, Roche KW, and Anggono V. (2020). Regulation of NMDA glutamate receptor functions by the GluN2 subunits. J. Neurochem 154, 121–143. [PubMed: 31978252]

Wang X, Zhao Y, Zhang X, Badie H, Zhou Y, Mu Y, Loo LS, Cai L, Thompson RC, Yang B, et al. (2013). Loss of sorting nexin 27 contributes to excitatory synaptic dysfunction by modulating glutamate receptor recycling in Down's syndrome. Nat. Med 19, 473–480. [PubMed: 23524343]

Willsey AJ, Morris MT, Wang S, Willsey HR, Sun N, Teerikorpi N, Baum TB, Cagney G, Bender KJ, Desai TA, et al. (2018). The Psychiatric Cell Map Initiative: A Convergent Systems Biological Approach to Illuminating Key Molecular Pathways in Neuropsychiatric Disorders. Cell 174, 505–520. [PubMed: 30053424]

Won S, Incontro S, Nicoll RA, and Roche KW (2016). PSD-95 stabilizes NMDA receptors by inducing the degradation of STEP61. Proc. Natl. Acad. Sci. USA 113, E4736–E4744. [PubMed: 27457929]

Won S, Levy JM, Nicoll RA, and Roche KW (2017). MAGUKs: multifaceted synaptic organizers. Curr. Opin. Neurobiol 43, 94–101. [PubMed: 28236779]

Wyllie DJ, Livesey MR, and Hardingham GE (2013). Influence of GluN2 subunit identity on NMDA receptor function. Neuropharmacology 74, 4–17. [PubMed: 23376022]

XiangWei W, Jiang Y, and Yuan H. (2018). De Novo Mutations and Rare Variants Occurring in NMDA Receptors. Curr. Opin. Physiol 2, 27–35. [PubMed: 29756080]

Yashiro K, and Philpot BD (2008). Regulation of NMDA receptor subunit expression and its implications for LTD, LTP, and metaplasticity. Neuropharmacology 55, 1081–1094. [PubMed: 18755202]

Yuan H, Hansen KB, Zhang J, Pierson TM, Markello TC, Fajardo KV, Holloman CM, Golas G, Adams DR, Boerkoel CF, et al. (2014). Functional analysis of a de novo GRIN2A missense mutation associated with early-onset epileptic encephalopathy. Nat. Commun 5, 3251. [PubMed: 24504326]

Zhou Q, and Sheng M. (2013). NMDA receptors in nervous system diseases. Neuropharmacology 74, 69–75. [PubMed: 23583930]

Zoghbi HY, and Bear MF (2012). Synaptic dysfunction in neurodevelopmental disorders associated with autism and intellectual disabilities. Cold Spring Harb. Perspect. Biol 4, a009886.

Highlights

- The epilepsy-associated variant GluN2A-S1459G causes NMDAR trafficking defects
- GluN2A-S1459G disrupts NMDAR interactions and leads to reduced mEPSC frequency
- GluN2A is phosphorylated by CaMKII at S1459, which is regulated by neuronal activity
- GluN2A-S1459 phosphorylation dictates binding to PDZ domain-containing proteins

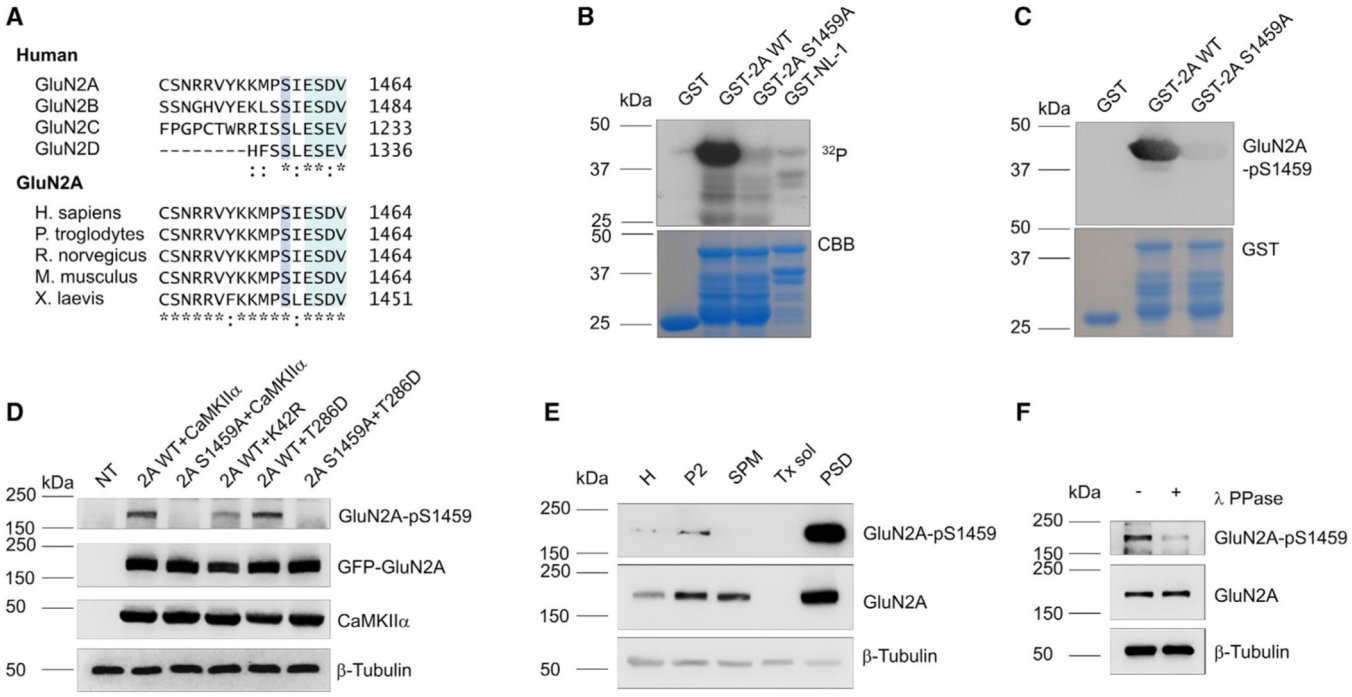

Figure 1. GluN2A-S1459 Is Phosphorylated by CaMKIIα

(A) Alignment of the extreme CTD of the 4 GluN2 human subunits (top) and of the GluN2A subunit in several species (bottom), highlighting the conserved S1459 residue (blue) and its proximity to the PDZ-binding domain (green).

(B and C) *In vitro* kinase assays using purified CaMKIIα and GST-GluN2A CTD (WT or S1459A) were performed. Total protein was visualized by Coomassie Brilliant Blue (CBB) protein staining.

(B) Autoradiography analysis of GST fusion proteins that were incubated with [γ-^{32}P]ATP.

(C) Analysis of GluN2A-S1459 phosphorylation by immunoblotting using the phosphospecific antibody.

(D) GFP-tagged GluN2A (WT or S1459A) was co-expressed with GluN1 and CaMKIIα (WT, K42R, or T286D) in HEK293T cells, and phosphorylation of GluN2A-S1459 was probed by immunoblotting.

(E) Adult mouse brains were fractionated and probed for endogenous phosphorylation of GluN2A-S1459.

(F) PSD fractions from adult mice were treated with l-phosphatase for 1 h at 37°C, to test antibody specificity. All of the experiments were performed independently 3 times.

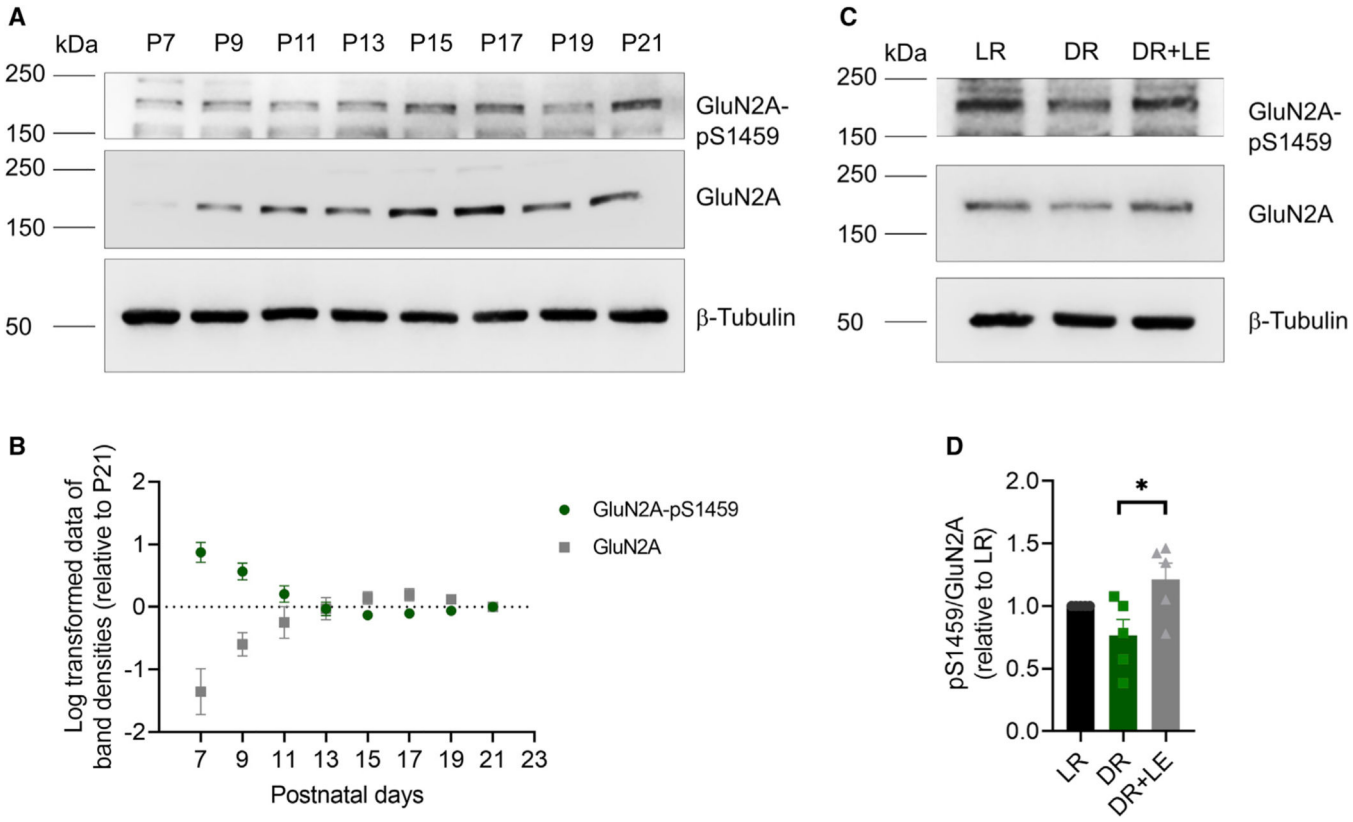

Figure 2. GluN2A-S1459 Phosphorylation Is Dynamically Regulated

(A and B) Developmental profile of GluN2A-S1459 phosphorylation. Brains of WT mice were collected at the indicated ages (postnatal days 7–21) and fractionated. Twenty mg of protein from the PSD fractions were resolved in SDS-PAGE, and the levels of phosphorylated GluN2A-S1459, total GluN2A, and tubulin were analyzed using immunoblotting. Band density was measured and values were normalized to tubulin and total GluN2A. The data are represented as means ± SEMs of log transformed values of normalized band densities (n = 4).

(C and D) Primary visual cortices from P26 animals subjected to a dark-rearing paradigm (LR, normal light/dark cycle; DR, dark reared from P21 to P26; DR + LE, dark reared from P21 to P26 with 2 h of exposure to light before euthanasia) were fractionated and the SPM fraction analyzed using immunoblotting. The data are represented as means ± SEMs (n = 5; 1-way ANOVA, followed by Sidak's multiple comparisons test; *statistically different from DR, p = 0.0109).

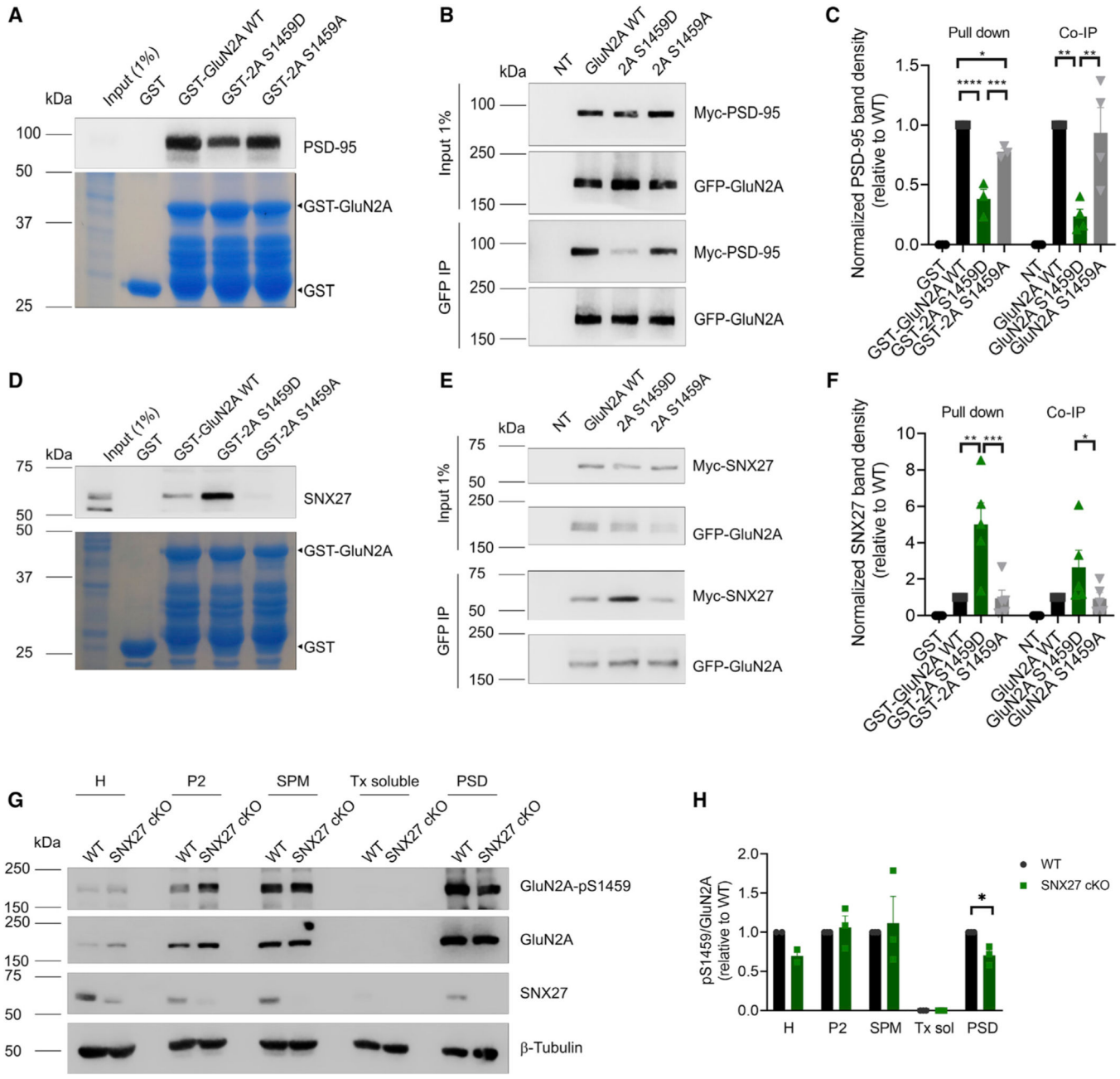

Figure 3. The Phosphorylation State of GluN2A-S1459 Affects Receptor Interactions with PDZ Domain-Containing Proteins

(A–C) Phosphorylation of GluN2A-S1459 reduces the binding to PSD-95.

(A) GST-GluN2A CTD fusion proteins (WT, S1459D, and S1459A) were incubated with P2 fractions from adult mouse brains. The samples were resolved by SDS-PAGE and probed for PSD-95 by western blot. Total protein was visualized with CBB staining.

(B) GFP-tagged GluN2A (WT, S1459D, or S1459A) was co-expressed with GluN1 and Myc-PSD-95. Co-IPs were performed, and samples resolved in SDS-PAGE and analyzed by western blot.

(C) The data are represented as means ± SEMs (n = 3; 1-way ANOVA followed by Sidak's multiple comparisons test; *significantly different from WT).
(D–F) Phosphorylation of GluN2A-S1459 modulates receptor interactions with SNX27.
(D) GST-GluN2A fusion proteins (as in A) were incubated with total homogenate from adult mouse brains. The samples were resolved by SDS-PAGE and probed for SNX27 using western blot. Total protein was visualized with CBB staining.
(E) NMDAR subunits (as in B) were co-expressed with Myc-SNX27 in HEK293T cells. Co-IPs were performed and samples analyzed by western blot.
(F) The data are represented as means ± SEMs (n = 5; 1-way ANOVA followed by Dunnett's or Sidak's multiple comparisons tests; *significantly different from WT or S1459D).
(G and H) Adult brains from WT or CRE-expressing LoxP-SNX27 mice were fractionated and the level of phosphorylated GluN2A-S1459 assessed using immunoblot, quantified and normalized to total GluN2A. The data are represented as means ± SEMs (n = 3; Student's t test; *significantly different from WT [CRE^{-}], p = 0.0126).

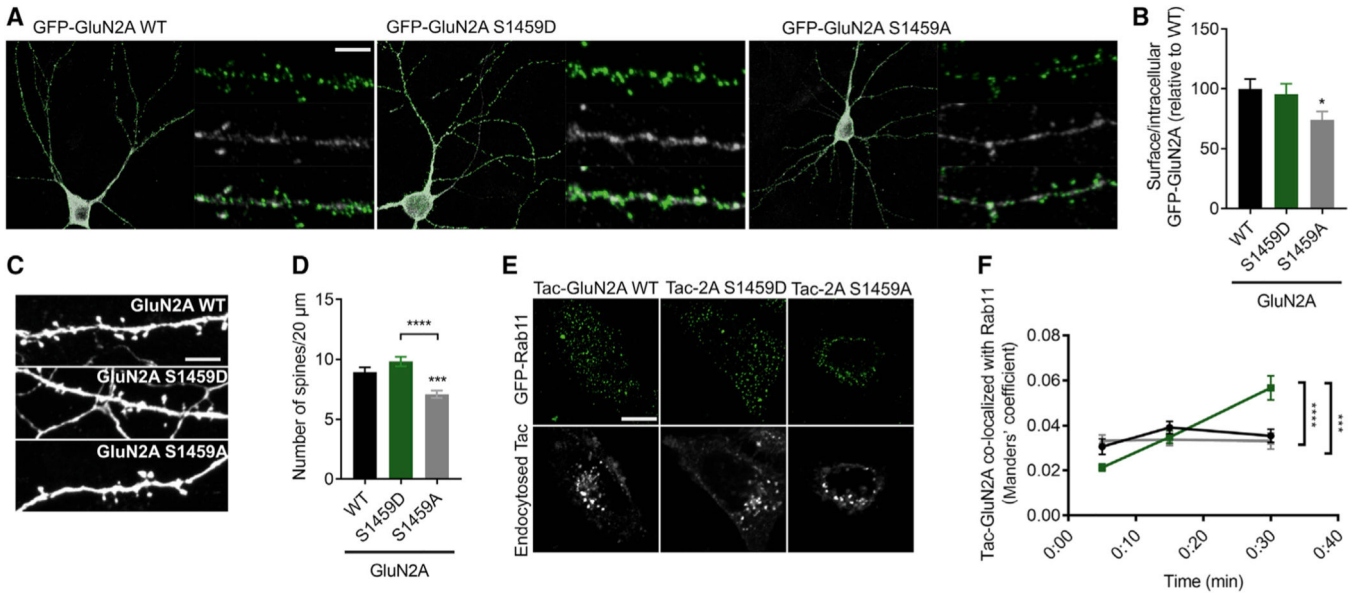

Figure 4. Phosphorylation of GluN2A-S1459 Modulates Receptor Surface Expression

(A and B) DIV13 rat hippocampal neurons were transfected with GFP-tagged GluN2A subunits, as indicated. At DIV17, surface (green) and intracellular (white) receptors were labeled. Coverslips were analyzed in a Zeiss LSM800 confocal microscope and quantifications were performed using the Metamorph software. The data were plotted as a ratio of surface/intracellular receptors (relative to WT) and represented as means ± SEMs (n = 4–5; 1-way ANOVA, followed by Dunnett's multiple comparisons test; *significantly different from WT, $p = 0.0351$).

(C and D) Hippocampal neurons were co-transfected with GluN2A constructs (as in A) and pCAG-GFP to allow visualization of the entire neuron. Spine density was analyzed using a Zeiss LSM800 microscope. The data are expressed as the number of spines per 20 µm dendrite and represented as means ± SEMs (n = 4–5; 1-way ANOVA, followed by Dunnett's or Sidak's multiple comparisons test; *significantly different from WT, $p = 0.0005$ or S1459D, $p < 0.0001$).

(E and F) HeLa cells expressing Tac-GluN2A (WT, S1459D, or S1459A) and GFP-Rab11 were subjected to 5–30 min of endocytosis. Cells were imaged using a Zeiss LSM800 microscope and then analyzed for co-localization between internalized Tac-GluN2A and Rab11. The data are expressed as the Manders' co-efficient of the fraction of Tac-GluN2A colocalizing with GFP-Rab11 and represented as means ± SEMs (n = 3; 2-way ANOVA, followed by Dunnett's multiple comparisons test; S1459D 30 min compared to 5 min, $p < 0.0001$; 2-way ANOVA, followed by Tukey's multiple comparisons test; *significantly different from WT 30 min, $p < 0.0001$, or S1459A 30 min, $p < 0.0001$). Scale bar, 10 µm.

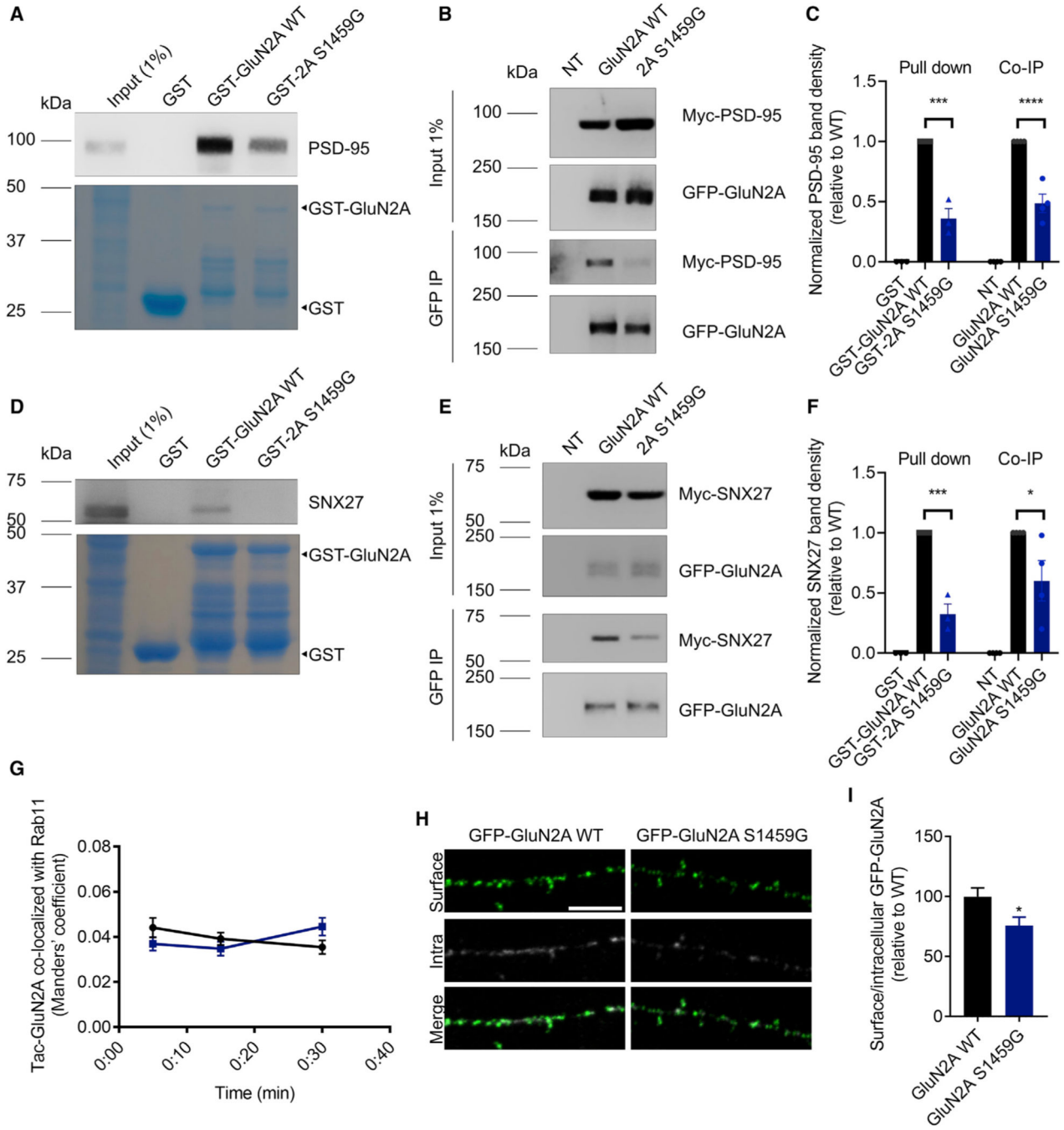

Figure 5. The Epilepsy Variant GluN2A-S1459 Impairs GluN2A PDZ Ligand-Mediated Interactions and Trafficking

(A–F) GluN2A-S1459G has reduced binding to PSD-95 (A–C) and SNX27 (D–F). Pull downs and coIPs were performed as in Figure 3, with the GluN2A WT or the GluN2A-S1459G mutant.

(A) Pull-down assay.

(B) Co-IP experiment.

(C) Quantification of band densities in (A) and (B). The data are represented as means ± SEMs (n = 3–4; 1-way ANOVA, followed by Dunnett's multiple comparisons test; *significantly different from WT, p = 0.0002 [pull down]; p < 0.0001 [co-IP].
(D) Pull-down assay.
(E) Co-IP experiment.
(F) Quantification of band densities in (C) and (D). The data are represented as means ± SEMs (n = 3–4; 1-way ANOVA, followed by Dunnett's multiple comparisons test; *significantly different from WT, p = 0.0001 [pull down]; p = 0.0310 [co-IP]).
(G) HeLa cells expressing Tac-GluN2A (WT or S1459G) and GFP-Rab11 were treated and analyzed as in Figure 4. The data are represented as means ± SEMs (n = 3).
(H and I) DIV13 rat hippocampal neurons were transfected with GFP-GluN2A subunits, as indicated, and surface/intracellular receptors labeled and analyzed as in Figure 5. The data are plotted as a ratio of surface/intracellular receptors (relative to WT) and represented as means ± SEMs (n = 5; Student's t test; *significantly different from WT, p = 0.0197). Scale bar, 5 μm.

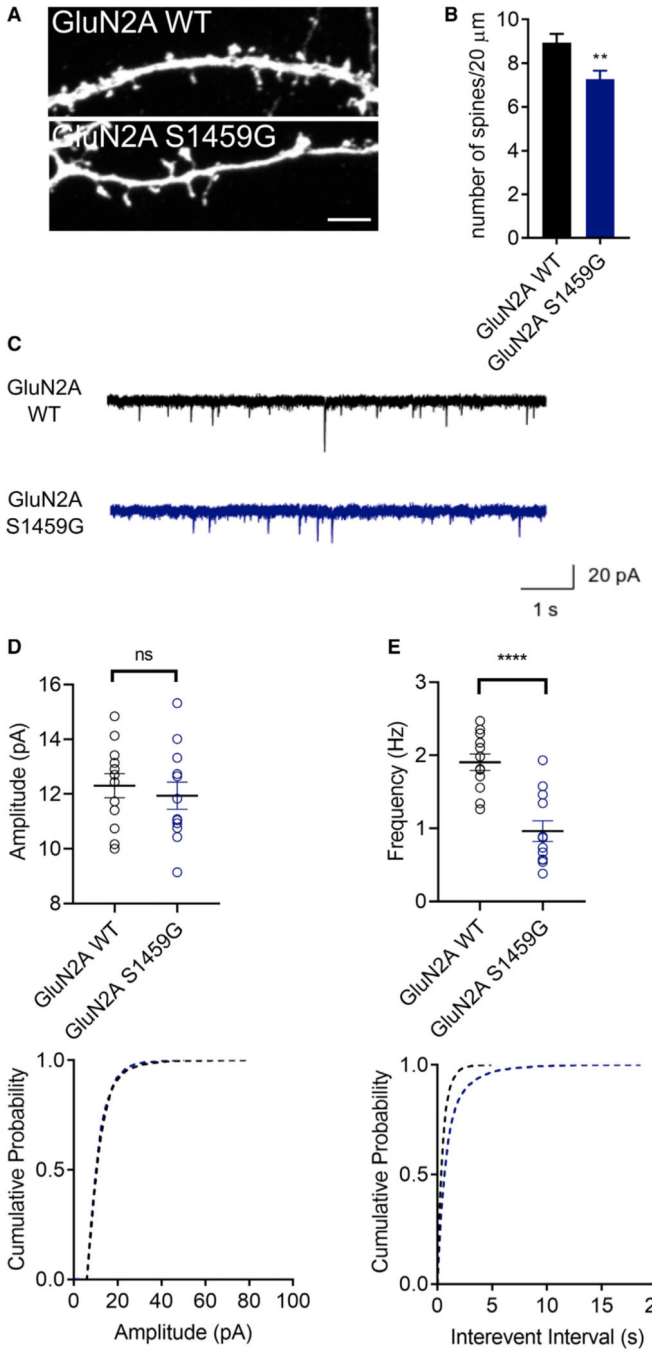

Figure 6. Neurons Expressing the Epilepsy Variant GluN2A-S1459G Have Compromised Neuronal Activity

(A and B) Hippocampal neurons were co-transfected with GluN2A constructs (as in Figure 5H) and pCAG-GFP. The spine density was analyzed using a Zeiss LSM800 microscope. The data are expressed as the number of spines per 20 µm and represented as means ± SEMs (n = 5; Student's t test; *significantly different from WT, p = 0.003).

(C) Representative mEPSC traces recorded in cultured hippocampal neurons expressing either GluN2A WT or S1459G.

(D) mEPSC mean amplitude and cumulative probability plots of mEPSC amplitude. The bar graph indicates means ± SEMs (n = 12 cells from 3 independent cultures; Student's t test). (E) mEPSC mean frequency and cumulative probability plots of mEPSC interevent intervals (n = 12 cells from 3 independent cultures; Student's t test; *significantly different from WT, $p < 0.0001$).

KEY RESOURCES TABLE

REAGENT or RESOURCE	SOURCE	IDENTIFIER
Antibodies		
Anti-CaMKIIα	Sigma-Aldrich	Cat#C265; RRID: AB_258808
Anti-GFP (rabbit - for Co-IP and ICC)	Thermo Fisher	Cat#A11122; RRID: AB_221569
Anti-GFP (mouse - for WB)	NeuroMab	Cat#N86/8; RRID: AB_2313651
Anti-GFP (chicken - for ICC)	Thermo Fisher	Cat#A10262; RRID: AB_2534023
Anti-GluN2A	Sigma-Aldrich	Cat#M264; RRID: AB_260485
Anti-Myc	Cell Signaling Technology	Cat#9B11; RRID: AB_823474
Anti-phosphoS1459	New England Peptide; This study	N/A
Anti-PSD-95	NeuroMab	Cat#73–028, RRID: AB_10698024
Anti-SNX27	New England Peptide; This study	N/A
Anti-Tac	ATCC	Cat#7G7
Anti-β-Tubulin III	Sigma-Aldrich	Cat#T2200; RRID: AB_262133
Anti-Mouse IgG HRP-linked	GE Healthcare	Cat#NA931; RRID: AB_772210
Anti-Rabbit IgG HRP-linked	GE Healthcare	Cat#NA934; RRID: AB_772206
Anti-rabbit Alexa Fluor 488	Thermo Fisher	Cat#A11034; RRID: AB_2576217
Anti-chicken Alexa Fluor 555	Thermo Fisher	Cat#A21437; RRID: AB_2535858
Anti-mouse Alexa Fluor 555	Thermo Fisher	Cat#A21422; RRID: AB_2535844
Anti-mouse Alexa Fluor 633	Thermo Fisher	Cat#A21052; RRID: AB_2535719
Chemicals, Peptides, and Recombinant Proteins		
Lipofectamine 2000	Thermo Fisher	Cat#11668019
Protease inhibitor mixture	Roche	Cat#11697498001
Phosphatase inhibitor mixture II	Sigma-Aldrich	Cat#P5726
Phosphatase inhibitor mixture III	Sigma-Aldrich	Cat#P0044
Protein A-Sepharose	Sigma-Aldrich	Cat#P3391
Glutathione Sepharose 4B	GE Healthcare	Cat#14–0756-05
Experimental Models: Cell Lines		

REAGENT or RESOURCE	SOURCE	IDENTIFIER
Human embryonic kydney (HEK) 293T	ATCC	Cat#CRL11268; RRID:CVCL_1926
HeLa	ATCC	Cat#CCL-2; RRID: CVCL_0030
Experimental Models: Organisms/Strains		
Rat: Sprague Dawley	Envigo	Cat#002
Mouse: C57BL/6J	The Jackson Laboratory	Cat#000664
Mouse: FVB/N-Tg(Thy1-cre)1Vln/J	The Jackson Laboratory	Cat#006143
Mouse: B6.Cg-Tg(ACTFLPe)9205Dym/J	The Jackson Laboratory	Cat#005703
Mouse: C57BL/6N-*Snx27*$^{tm1a(KOMP)Wtsi}$/MbpMmucd	UC Davis KOMP	Cat#049799-UCD; RRID:MMRRC_049799-UCD
Oligonucleotides		
GluN2A-S1459A Fwd primer: CAAGAAAATGCCTGCTA TCGAATCTGATG	This study	N/A
GluN2A-S1459A Rvs primer: CATCAGATTCGATAGCAGGC ATTTTCTTG	This study	N/A
GluN2A-S1459D Fwd primer: CAAGAAAATGCCTGATATC GAATCTGATG	This study	N/A
GluN2A-S1459D Rvs primer: CATCAGATTCGATATCAGGCATTTTCTTG	This study	N/A
GluN2A-S1459G Fwd primer: CAAGAAAATGCCTGGTAT CGAATCTGATG	This study	N/A
GluN2A-S1459G Rvs primer: CATCAGATTCGATACCAGGCAT TTTCTTG	This study	N/A
Recombinant DNA		
pRK5-GFP-GluN2A	Dr. Stefano Vicini (Georgetown University, DC)	N/A
pGEX4-GST-GluN2A CTD	Sanz-Clemente et al., 2010	N/A
pRK5-Tac-GluN2A CTD	Lavezzari et al., 2004	N/A
GFP-Rab11	Dr. Juan Bonifacino (NIH, MD)	N/A
pCAG-CaMKIIα WT	Dr. Roger Nicoll (UCSF, CA)	N/A
pCAG-CaMKIIα K42R	Dr. Roger Nicoll (UCSF, CA)	N/A
pCAG-CaMKIIα T286D	Dr. Roger Nicoll (UCSF, CA)	N/A
pRK5-Myc-PSD-95	Sanz-Clemente et al. (2010)	N/A
pRK5-Myc-SNX27	Clairfeuille et al. (2016)	N/A
pRK5-GluN1 (untagged)	Sanz-Clemente et al. (2010)	N/A

REAGENT or RESOURCE	SOURCE	IDENTIFIER
pCAG-GFP	Liu et al. (2017)	N/A
Software and Algorithms		
BioRender (Graphical abstract)	Biorender.com	RRID: SCR_018361
Image-J	NIH	RRID: SCR_003070
Inkscape1.0	Inkscape	RRID: SCR_014479
GraphPad Prism 8	GraphPad	RRID: SCR_002798
Metamorph	Molecular Devices	RRID: SCR_002368
Adobe Photoshop CC 2018	Adobe	RRID: SCR_014199